

2024

Re-Evaluating Hydrogen Sulfide as a Sink for Cadmium and Zinc in the Oxidic to Suboxic Upper Water Column of the Pacific Ocean

N. R. Buckley
Old Dominion University, nbuck005@odu.edu

E. E. Black
University of Rochester

J. A. Kenyon
Woods Hole Oceanographic Institution

N. T. Lanning
Texas A&M University

M. Sieber
University of South Florida

See next page for additional authors

Follow this and additional works at: https://digitalcommons.odu.edu/oeas_fac_pubs



Part of the [Biogeochemistry Commons](#), and the [Oceanography Commons](#)

Original Publication Citation

Buckley, N. R., Black, E. E., Kenyon, J. A., Lanning, N. T., Sieber, M., Conway, T. M., Fitzsimmons, J. N., & Cutter, G. A. (2024). Re-evaluating hydrogen sulfide as a sink for cadmium and zinc in the oxidic to suboxic upper water column of the Pacific Ocean. *Global Biogeochemical Cycles*, 38(3), 1-18, Article e2023GB007881. <https://doi.org/10.1029/2023GB007881>

This Article is brought to you for free and open access by the Ocean & Earth Sciences at ODU Digital Commons. It has been accepted for inclusion in OES Faculty Publications by an authorized administrator of ODU Digital Commons. For more information, please contact digitalcommons@odu.edu.

Authors

N. R. Buckley, E. E. Black, J. A. Kenyon, N. T. Lanning, M. Sieber, T. M. Conway, J. N. Fitzsimmons, and G. A. Cutter

Global Biogeochemical Cycles®





RESEARCH ARTICLE

10.1029/2023GB007881

Special Section:

The U.S. GEOTRACES Pacific Meridional Transect (GP15)

Re-Evaluating Hydrogen Sulfide as a Sink for Cadmium and Zinc in the Oxic to Suboxic Upper Water Column of the Pacific Ocean

N. R. Buckley¹ , E. E. Black² , J. A. Kenyon³, N. T. Lanning⁴, M. Sieber⁵ , T. M. Conway⁵, J. N. Fitzsimmons⁴ , and G. A. Cutter¹

¹Department of Ocean and Earth Sciences, Old Dominion University, Norfolk, VA, USA, ²Department of Earth and Environmental Sciences, University of Rochester, Rochester, NY, USA, ³MIT-WHOI Joint Program in Chemical Oceanography, Woods Hole Oceanographic Institution, Woods Hole, MA, USA, ⁴Department of Oceanography, Texas A&M University, College Station, TX, USA, ⁵College of Marine Science, University of South Florida, St. Petersburg, FL, USA

Key Points:

- Sulfide concentrations are too low to support the 0.1 nM deficit observed in dissolved Cd in the low oxygen North Pacific
- Assimilatory and dissimilatory sulfate reduction can explain the dissolved metal deficits in the shallow Eastern Tropical South Pacific OMZ
- Particulate sulfide maxima coincide with the largest apparent dissolved Cd deficits observed in the subsurface waters of the Pacific Ocean

Correspondence to:

N. R. Buckley and G. A. Cutter,
nbuckley@odu.edu;
gcutter@odu.edu

Citation:

Buckley, N. R., Black, E. E., Kenyon, J. A., Lanning, N. T., Sieber, M., Conway, T. M., et al. (2024). Re-evaluating hydrogen sulfide as a sink for cadmium and zinc in the oxic to suboxic upper water column of the Pacific Ocean. *Global Biogeochemical Cycles*, 38, e2023GB007881. <https://doi.org/10.1029/2023GB007881>

Received 12 JUN 2023

Accepted 27 FEB 2024

Author Contributions:

Conceptualization: N. R. Buckley, G. A. Cutter

Formal analysis: N. R. Buckley

Funding acquisition: T. M. Conway, J. N. Fitzsimmons, G. A. Cutter

Investigation: N. R. Buckley, E. E. Black, J. A. Kenyon, N. T. Lanning, M. Sieber

Writing – original draft: N. R. Buckley, G. A. Cutter

Writing – review & editing:

N. R. Buckley, M. Sieber, T. M. Conway, J. N. Fitzsimmons, G. A. Cutter

© 2024. The Authors.

This is an open access article under the terms of the [Creative Commons Attribution-NonCommercial-NoDerivs License](#), which permits use and distribution in any medium, provided the original work is properly cited, the use is non-commercial and no modifications or adaptations are made.

Abstract Hydrogen sulfide is produced by heterotrophic bacteria in anoxic waters and via carbonyl sulfide hydrolysis and phytoplankton emissions under oxic conditions. Apparent losses of dissolved cadmium (dCd) and zinc (dZn) in oxygen minimum zones (OMZs) of the Atlantic and Pacific Oceans have been attributed to metal-sulfide precipitation formed via dissimilatory sulfate reduction. It has also been argued that such a removal process could be a globally important sink for dCd and dZn. However, our studies from the North Pacific OMZ show that dissolved and particulate sulfide concentrations are insufficient to support the removal of dCd via precipitation. In contrast, apparent dCd and dZn deficits in the eastern tropical South Pacific OMZ do reside in the oxycline with particulate sulfide maxima, but they also coincide with the secondary fluorescence maxima, suggesting that removal via sulfide precipitation may be due to a combination of dissimilatory and assimilatory sulfate reduction. Notably, dCd loss via precipitation with sulfide from assimilatory reduction was found in upper oxic waters of the North Pacific. While dissimilatory sulfate reduction may explain local dCd and dZn losses in some OMZs, our evaluation of North Pacific OMZs demonstrates that dCd and dZn losses are unlikely to be a globally relevant sink. Nevertheless, metal sulfide losses due to assimilatory sulfate reduction in surface waters should be considered in future biogeochemical models of oceanic Cd (and perhaps Zn) cycling.

Plain Language Summary The Pacific Ocean hosts multiple oxygen minimum zones (OMZs), chiefly in the Northeast Pacific and the Eastern Tropical Pacific. Despite studies identifying apparent deficits of dissolved cadmium (dCd) and zinc (dZn) relative to established relationships with macronutrients within OMZ waters and hypothesizing that precipitation of insoluble metal sulfides is the cause, our measurements of particulate metal sulfides are too small to support this removal hypothesis. However, we demonstrate that a possible loss of dCd related to metal-sulfide precipitation is actually more likely in the surface oxygenated ocean rather than in OMZ waters.

1. Introduction

Dissolved trace elements such as iron, cadmium, and zinc are essential micronutrients for the growth of phytoplankton in the ocean, influencing carbon cycling and global climate (Bruland & Lohan, 2006; Morel et al., 2003). In seawater, dissolved cadmium (Cd) and zinc (Zn) have nutrient-like distributions (Boyle et al., 1976; Bruland et al., 1978) driven by phytoplankton assimilation in surface waters and accumulation in deeper waters due to cellular regeneration and advection of nutrient-rich water masses from the Southern Ocean (Baars et al., 2014; Bruland & Lohan, 2006; Vance et al., 2017). Therefore, one-dimensional dissolved Cd and Zn profiles resemble those of the macronutrients phosphate (PO_4^{3-}) and silicate ($\text{Si}(\text{OH})_4$), respectively, and thus broadly exhibit a linear relationship to one another (Bruland & Lohan, 2006). From this global linear metal:nutrient relationship, anomalies from the canonical dissolved Cd: PO_4^{3-} (cadmium-to-phosphate) and Zn:Si (zinc-to-silicate) relationships can be expressed using the ‘star’ convention (Cd^* and Zn^*):

$$\text{Cd}^* = \text{Cd}_{\text{measured}} - \text{PO}_4^{3-}_{\text{measured}} \times \frac{\text{Cd}_{\text{deep}}}{\text{PO}_4^{3-}_{\text{deep}}} \quad (1)$$

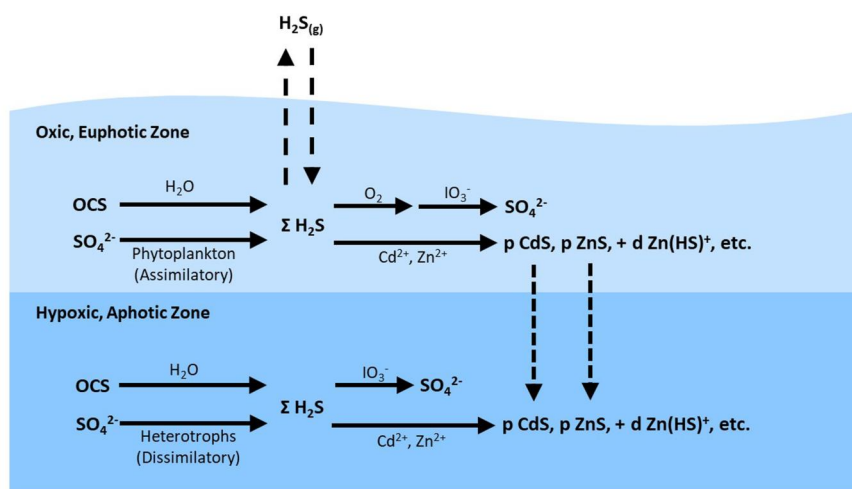


Figure 1. Proposed biogeochemical cycle of hydrogen sulfide in the surface ocean and underlying oxygen minimum zone (OMZ). $\Sigma\text{H}_2\text{S}$ represents free, uncomplexed sulfide ($\text{H}_2\text{S}_{\text{aq}} + \text{HS}^- + \text{S}^{2-}$). $\Sigma\text{H}_2\text{S}$ is produced via OCS hydrolysis, assimilatory sulfate reduction, dissimilatory sulfate reduction, or atmospheric interaction. $\Sigma\text{H}_2\text{S}$ can then react with dissolved metals to form dissolved metal-sulfide complexes, particulate metal sulfides, or undergo oxidation to sulfate. These reaction pathways are shown as solid lines while dashed lines represent fluxes. Total dissolved sulfide is presented by the sum of $\Sigma\text{H}_2\text{S}$ and dissolved metal-sulfide complexes ($\text{d Zn}(\text{HS})^+$, etc.), whereas particulate acid-volatile sulfide is represented by the particulate metal-sulfide complexes (p CdS , p ZnS , p NiS , etc.). However, it should be noted that some OMZs, like the eastern tropical South Pacific, have OMZs that shoal into euphotic waters, and thus sulfide could be produced by both dissimilatory and assimilatory sulfate reduction.

$$\text{Zn}^* = \text{Zn}_{\text{measured}} - \text{Si}_{\text{measured}} \times \frac{\text{Zn}_{\text{deep}}}{\text{Si}_{\text{deep}}} \quad (2)$$

where $\text{Cd}_{\text{measured}}$ and $\text{Zn}_{\text{measured}}$ are the dissolved metal concentrations, $\text{PO}_4^{3-}_{\text{measured}}$ and $\text{Si}_{\text{measured}}$ are the measured nutrient concentrations, and where the deep water metal:macronutrient ratios, $\frac{\text{Cd}_{\text{deep}}}{\text{PO}_4^{3-}_{\text{deep}}}$ and $\frac{\text{Zn}_{\text{deep}}}{\text{Si}_{\text{deep}}}$, can be set locally or globally (Conway & John, 2014; Janssen et al., 2014). Such Cd^* and Zn^* anomalies thus represent local or water-mass specific deviations of these metal-nutrient relationships from the whole ocean values, where positive values indicate an apparent surplus and negative values indicate an apparent metal deficit compared to their paired macronutrients. However, it is important to note that while Cd^* or Zn^* are useful in indicating relative difference in the ratio of the metals to the macronutrients in certain samples or water masses, they do not provide any information on the reason or mechanism for this decoupling nor do they explicitly support local loss or gain of the element.

Using Cd^* and Zn^* anomalies, the oxygen minimum zones (OMZ; $<50 \mu\text{mol kg}^{-1}$) of the North Pacific (Conway & John, 2015b; Janssen & Cullen, 2015; Janssen et al., 2014, 2019) and the North and South Atlantic (Conway & John, 2014, 2015a; Guinoiseau et al., 2018, 2019; Janssen et al., 2014) have been identified as regions with lower observed dCd and dZn concentrations than predicted from macronutrient concentrations. It was hypothesized (Janssen & Cullen, 2015) that this loss could be explained by the precipitation of insoluble metal sulfides produced by dissimilatory sulfate reduction within anoxic microenvironments of sinking organic particles in the OMZ (Figure 1). This mechanism was postulated to serve as a major sink of dCd and dZn from the global ocean (Conway & John, 2015a; Guinoiseau et al., 2019; Janssen & Cullen, 2015; Janssen et al., 2014; Xie, Rehkämper, et al., 2019), but recent work suggests that the explanation for the apparent dissolved metal deficits in low oxygen environments is still being disputed (e.g., de Souza et al., 2022; Janssen et al., 2019; Sieber, Lanning, Bunnell, et al., 2023).

Initially, the sulfide precipitation hypothesis was supported by the apparent decoupling of Cd and PO_4^{3-} for OMZs globally with deviations of up to $-0.3 \text{ nmol kg}^{-1}$ dissolved Cd^* (Conway & John, 2015a; Guinoiseau et al., 2019; Janssen et al., 2014; Xie, Rehkämper, et al., 2019); along with enrichment of isotopically light Cd particles found at OMZ depths in the North Pacific (Janssen et al., 2019) and North Atlantic (Conway &

John, 2015a; Janssen et al., 2014) that is associated with CdS precipitation (Guinoiseau et al., 2018; Schmitt et al., 2009; Yang et al., 2015). However, evidence for zinc sulfide (ZnS) removal within OMZs is more equivocal despite apparent dissolved Zn deficits previously documented within the North Pacific and Atlantic OMZs (Conway & John, 2014; Janssen & Cullen, 2015; Janssen et al., 2014). Instead, recent studies have focused on alternative explanations for relative dCd and dZn depletion in OMZs since several observations do not support this sulfide precipitation mechanism as a globally important phenomenon (e.g., Janssen et al., 2019; Ohnemus et al., 2016; Roshan & DeVries, 2021; Vance et al., 2019). These findings call into question previous interpretations such as light Cd in particles as evidence for Cd-sulfide removal (Janssen et al., 2019). However, it is important to note that most studies to date have not evaluated whether sufficient sulfide exists in the North Pacific OMZ to support the proposed metal-sulfide precipitation. In fact, only the ratios of insoluble particulate acid volatile sulfide (pAVS) to total particulate trace metals have been examined in the eastern tropical South Pacific (ETSP; Ohnemus et al., 2016) as well as benthic fluxes of dissolved iron and cadmium coupled with hydrogen sulfide concentrations from the Peruvian shelf (Plass et al., 2020; Schlosser et al., 2018; Xie, Rehkämper, et al., 2019).

Although sulfide is more commonly associated with low oxygen environments and is produced via dissimilatory sulfate reduction (Canfield et al., 2010), it is also produced in the fully oxic water column (Figure 1) via carbonyl sulfide (OCS) hydrolysis (Elliott et al., 1987) or by assimilatory sulfate reduction within phytoplankton (Walsh et al., 1994). This latter process likely dominates sulfide production in surface waters (Radford-Knoery & Cutter, 1994), but the net sulfide production depends on the biological species present and the concentration of dissolved free metals (Walsh et al., 1994). Consequently, any dissolved, uncomplexed sulfide produced by either of these mechanisms is available to react with metals to form dissolved metal-sulfide complexes or may undergo oxidation to sulfate (Jia-Zhong & Whitfield, 1986; Millero et al., 1987; Pos et al., 1997). Dissolved sulfide can also directly precipitate to form insoluble particulate metal monosulfides (e.g., CdS, ZnS, FeS, NiS) known as (pAVS; Radford-Knoery & Cutter, 1994). This pAVS term would be the particulate CdS and ZnS postulated to be in OMZs where dissolved metal deficits have been observed. However, the exact speciation of pAVS is unknown, although from a purely chemical argument regarding Cd versus Zn removal by sulfide precipitation, the more polarizable nature and larger ionic radius of the Cd²⁺ ion (“soft” acid) would have a higher affinity for “soft” sulfide ligands than the less polarizable (“harder”) Zn²⁺ ion (Pearson, 1963).

Taken together, arguments supporting a global significance of metal precipitation within OMZs have become increasingly tenuous in light of recent studies, limiting any potential impact from CdS and ZnS precipitation to the local or regional scale. Moreover, the recent re-assessment by de Souza et al. (2022) identified a signal of Cd loss within the oxycline of the shallow subsurface that is not confined to oxygen-deficient waters but ubiquitous throughout the tropics. Here, we present sulfide measurements alongside dissolved Cd and Zn concentrations in the upper water column of the North Pacific and the ETSP from US GEOTRACES GP15 and GP16 transects. The goal of this study is to evaluate whether enough sulfide exists to account for the dissolved metal deficits observed in the North Pacific OMZ, as proposed by Janssen and co-authors (Janssen & Cullen, 2015; Janssen et al., 2014), as well as to explore the relationship between sulfides and dissolved metals throughout the oxic to suboxic water column of the Pacific and parts of the North Atlantic Ocean.

2. Materials and Methods

2.1. Sampling Site

The US GEOTRACES GP15 Pacific Meridional Transect (hereafter referred to as GP15) was sampled between 56°N and 20°S along 152°W from 18 September to 24 November 2018, on board R/V *Roger Revelle*. Transect profiles of dissolved oxygen (Figure 2b) and total dissolved sulfide (TDS; Figure 2d) are shown for 16 stations, and small size fraction (0.8–51 μm) pAVS for 13 stations (Figure 2c) on GP15. For a closer examination of the coupling between Cd, Zn, and sulfide in the N. Pacific, four GP15 stations were used (Figure 3): Station 10 (42°N, 152°W), 12 (37°N, 152°W), 14 (32°N, 152°W), and 16 (27°N, 152°W).

The US GEOTRACES GP16 East Pacific Zonal Transect (hereafter referred to as GP16) was sampled between 77.4°W and 152°W along ~12°S from 25 October to 20 December 2013, on board R/V *Thomas G. Thompson*. Transect profiles of dissolved oxygen (Figure 4b) and small size fraction (0.8–51 μm) pAVS (Figure 4c) are shown for nine stations on the GP16 cruise. To examine the coupling more closely between Cd, Zn, and particulate sulfide in the ETSP, two stations were used (Figure 5): Station 5 (12°S, 78.2°W) and 9 (12°S, 89°W).

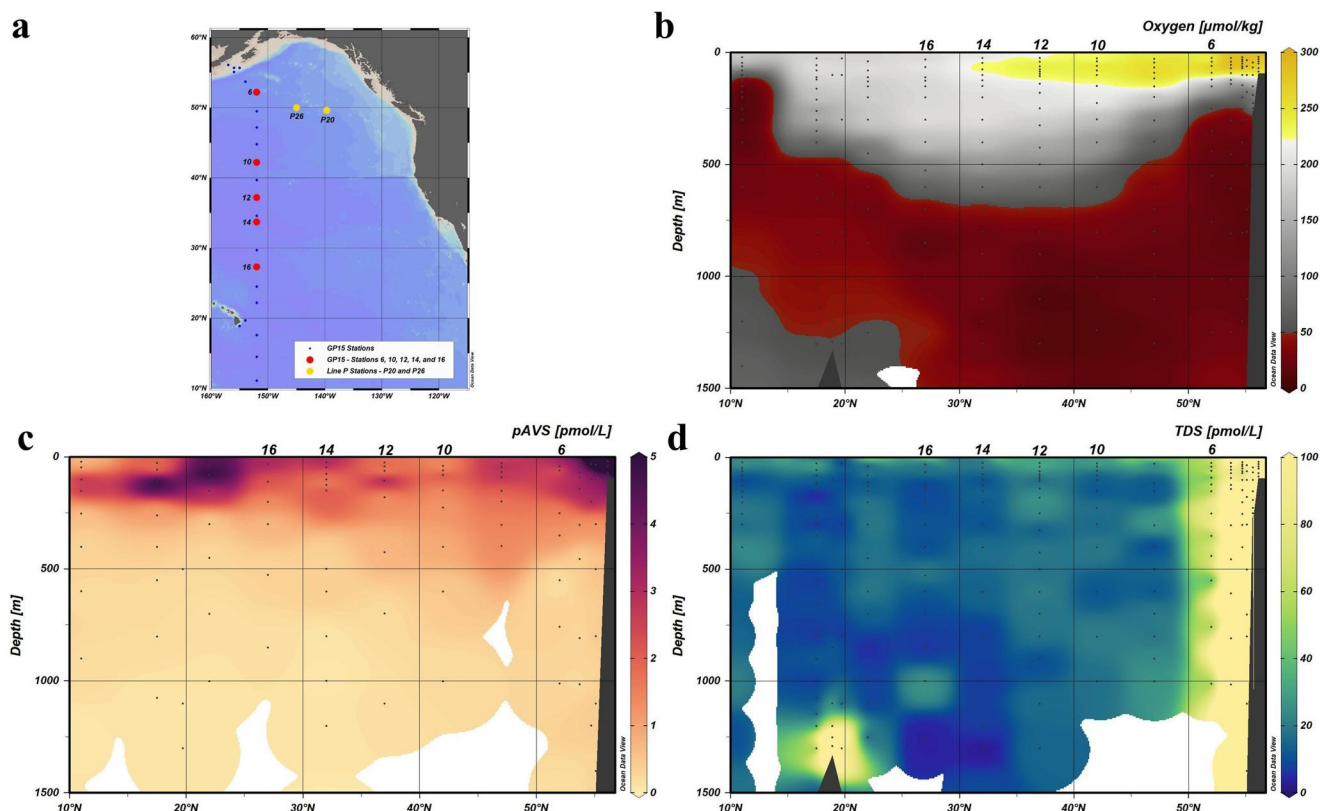


Figure 2. Sampling locations on the 2018 US GEOTRACES GP15 transect where Stations 6 (52°N, 152°W), 10 (42°N, 152°W), 12 (37°N, 152°W), 14 (32°N, 152°W), and 16 (27°N, 152°W) are shown as red dots in panel (a). Janssen et al. (2014) and Janssen and Cullen (2015) stations P20 (49.6°N, 139.7°W) and P26 (50°N, 145°W) are shown as yellow dots. Contoured transect profiles of dissolved oxygen (panel b), particulate acid-volatile sulfide (pAVS; panel c), and total dissolved sulfide (TDS; panel d) concentrations are shown with original data points shown as black dots. Station locations of interest are indicated above panels (b, c, and d). TDS concentrations occasionally exceeded 100 pmol L⁻¹, closer to the Alaskan shelf and Loihi hydrothermal plume. pAVS concentrations occasionally exceeded 5 pmol L⁻¹.

2.2. Seawater Sample Collection

GP15 and GP16 water samples were collected using the US GEOTRACES trace metal sampling system (Cutter & Bruland, 2012) with 24-12 L GO FLO bottles mounted on a trace metal clean carousel with CTD, oxygen, fluorometer, and transmissometer sensors. Trace metal clean sampling procedures were followed (Cutter et al., 2017) and bottles were pressurized with 6 psi air (GP15) or nitrogen (GP16). 1.5 L of seawater from each depth was pressure filtered directly through 0.2 μm AcroPak capsules and into 4 L polyethylene cubitainers for dissolved sulfide analyses (Radford-Knoery & Cutter, 1993). The cubitainers were then stored in a refrigerator and analyzed at sea within 8 hr. Seawater for dissolved Cd and Zn concentration analyses was filtered from the same GO FLO bottles into acid-cleaned 250 mL Texas A&M University (TAMU) and 2 L University of South Florida (USF) acid-cleaned Nalgene LDPE bottles. Filtered seawater samples were acidified shipboard to 0.024 M HCl (TAMU) or back in the lab to 0.012 M HCl (USF) using ultrapure HCl, and left for at least 6 months prior to analysis.

2.3. Particulate Sample Collection

Particulate sulfide samples were collected by P. Lam's sampling team using modified McLane in situ pumps with two mini-MULVFS filter holders (Bishop et al., 2012) each plumbed with their own flowmeter. One of the holders contained a 51 μm polyester mesh prefilter and particles collected on a 0.8 μm polyethersulfone Supor membrane filter (0.8–51 μm size fraction). The other filter holder contained the same prefilter but collected particles on a Whatman QMA quartz fiber filter (1–51 μm size fraction; Bishop et al., 2012). Excess seawater in the filter holders was removed using a vacuum pump within an hour of pump recovery. The Supor filters were then subsectioned in the onboard trace metal clean lab by P. Lam's (University of California, Santa Cruz) pump

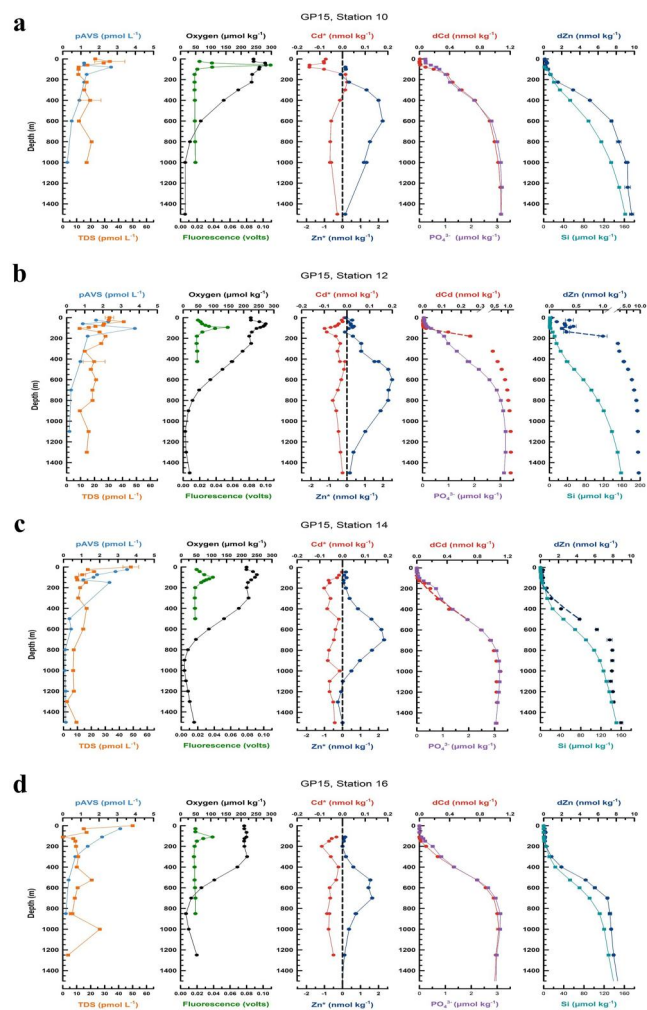


Figure 3. Vertical profiles of particulate acid-volatile sulfide, total dissolved sulfide (TDS), dissolved oxygen, fluorescence, derived Cd*, derived Zn*, dissolved Cd (dCd), phosphate (PO_4^{3-}), dissolved Zn (dZn), and silicate (Si) concentrations collected on the 2018 US GEOTRACES GP15 transect in the North Pacific with Station 10 (42.0°N, 152.0°W) shown in panel (a), Station 12 (37.0°N, 152°W) in panel (b), Station 14 (32.0°N, 152.0°W) in panel (c), and Station 16 (27°N, 152.0°W) in panel (d). Error bars on TDS data indicate one standard deviation above and below the mean for samples that were analyzed in triplicate.

pAVS for the small size fraction (0.8–51 μm) was determined at sea for both GP15 and GP16 samples using the Radford-Knoery and Cutter (1993) procedure. This method entails placing the frozen Supor filter into a gas stripping vessel with deionized water, acidifying to 1 M HCl, and then gas stripping, cryogenically trapped, and quantified using gas chromatography/flame photometric detection. This method has a particle detection limit of 0.2 pmol S, which corresponds to a relative detection limit of 0.004 pmol L^{-1} pAVS with an average filtered volume of 50 L. Particulate AVS samples were analyzed mostly in single analyses; however, previous studies report pAVS precision near 10% RSD (Cutter & Kluckhohn, 1999; Cutter & Radford-Knoery, 1991).

2.5. Determination of Dissolved Zn and Cd

Dissolved Zn and Cd concentrations were independently measured back on shore at both TAMU by isotope dilution via pico-SEAFast and ICP-MS, and at USF using a batch extraction method and isotope dilution

team and placed one-eighth of the filter subsamples in cryovials that were subsequently stored frozen at -80°C until analysis for pAVS. The whole Supor filters had between 100 and 1,100 L filtered through them, with an average of 400 L and thus an average effective volume of 50 L for the Supor subsample (12.5% of each filter). For particulate ^{234}Th samples, particles from the pre-filter were rinsed onto silver filters using 0.1 μm filtered seawater. Both the silver filter and 25 mm QMA subsample filter were measured on Risø Laboratories anti-coincidence beta counters. The entire QMA filters had between 300 and 1,540 L filtered through them, with an average filtration volume of 1,100 L and therefore an average effective volume of 43 L for a 25 mm QMA subsample (3.9% of each filter). It should be emphasized that the particulate concentrations in the study were calculated from the actual filter volumes for each sample, and not the average.

It is important to note that even though the small sized fraction (SSF; $<51 \mu\text{m}$) pAVS analyses were performed on a subsample of the Supor (0.8–51 μm) filter, and SSF ^{234}Th analyses were conducted on a subsample of the QMA (1–51 μm) filters, it is assumed that these filters are sampling a similar population of particles (Bishop et al., 2012). Therefore, pAVS results obtained from Supor filters can be related to ^{234}Th analyses acquired from the QMA filters, as was done by Black et al. (2019). Large sized fraction (LSF; $>51 \mu\text{m}$) particulate ^{234}Th activities were obtained from the Supor prefilter and used to estimate the unmeasured LSF pAVS flux (see discussion in Sections 3.2 and 3.3).

2.4. Determination of Dissolved and Particulate Sulfide

At sea, dissolved samples (only measured on GP15) were acidified to a pH of 1.6 with phosphoric acid and then gas stripped, cryogenically trapped, and quantified with gas chromatography/flame photometric detection using the method of Radford-Knoery and Cutter (1993). This quantifies TDS as free sulfide (hydrogen sulfide ions) plus metal-sulfide complexes with a 0.2 pmol S L^{-1} detection limit and precision of 13.7% RSD from duplicate and triplicate analyses. In addition to TDS, free sulfide was measured on all surface samples and some vertical profiles (e.g., GP15 Station 8 (47°N, 152°W)) where free sulfide was below the detection limits for all samples. It should be noted that free sulfide detection limits vary depending on the pH, temperature, and salinity of the solution. Using values from Station 8 (47°N, 152°W) as an example, detection of free sulfide was limited to 3 pmol L^{-1} with a pH of 7.92, a salinity of 32.3, and at 15°C. This suggests that TDS was metal-complexed, rather than existing as uncomplexed sulfide along the entire GP15 transect.

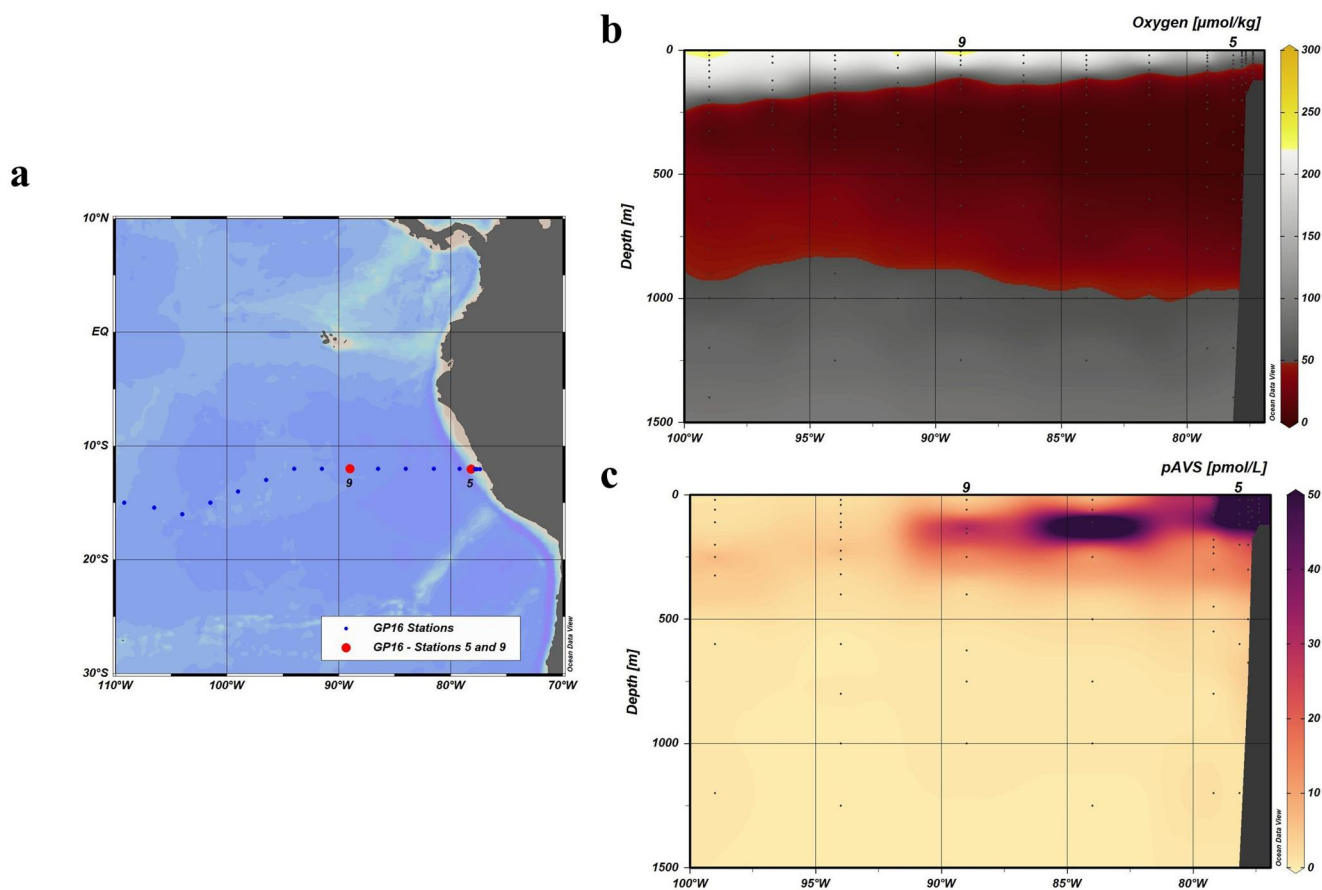


Figure 4. Sampling locations on the 2013 US GEOTRACES GP16 where Stations 5 (12.0°S, 78.2°W) and 9 (12.0°S, 89°W) are shown as red dots in panel (a). Contoured transect profiles of dissolved oxygen (panel b) and particulate acid volatile sulfide (pAVS; panel c) concentrations are shown with original data points shown as black dots. pAVS data are from Ohnemus et al. (2016) and occasionally exceeded 50 $\mu\text{mol L}^{-1}$ closer to the South American coast.

analysis by MC-ICP-MS. The methods of analysis at each institution have been described in detail previously (Conway et al., 2013; Jensen et al., 2020) with uncertainty on concentrations expressed as 2% (both institutions). Excellent agreement was found between the two labs (see Sieber, Lanning, Bian, et al., 2023; Sieber, Lanning, Bunnell, et al., 2023, Supporting Information). Dissolved metal concentrations were averaged from both institutions for each bottle depth for all samples except for surface Cd depths where the 4 L samples of USF provided better accuracy than the 250 mL samples used by TAMU, and when one institution had an obvious outlier (excluded from average). More details of methods used on GP15, and an intercomparison of the full GP15 section for Cd and Zn concentrations between three institutions can be found in Sieber et al. (Sieber, Lanning, Bian, et al., 2023; Sieber, Lanning, Bunnell, et al., 2023); the GP15 dZn and dCd data used here are a subset of the full sections reported in those publications.

2.6. Calculation of Dissolved Zn* and Cd*

Cd* and Zn* were calculated using Equations 1 and 2 following Janssen et al. (2014), Conway and John (2014), and Janssen and Cullen (2015). The $\frac{\text{Cd}_{\text{deep}}}{\text{PO}_4^{3-}_{\text{deep}}}$ represents the average deep water ratio of 0.35 $\text{nmol } \mu\text{mol}^{-1}$ taken from Janssen et al. (2014), and the $\frac{\text{Zn}_{\text{deep}}}{\text{Si}_{\text{deep}}}$ represents the average deep water ratio of 0.059 $\text{nmol } \mu\text{mol}^{-1}$ taken from Janssen and Cullen (2015). Studies in the North and South Pacific (Janssen et al., 2014; Sieber et al., 2019) in combination with GP15 data show that the deep Cd:PO₄³⁻ ratio is 0.35 mmol mol^{-1} throughout the deep Pacific (Sieber, Lanning, Bunnell, et al., 2023). This is similar to the globally relevant deep Zn:Si ratio (0.064 mmol mol^{-1}) and Cd:PO₄³⁻ ratio (0.33 mmol mol^{-1}) suggested by Vance et al. (2017) and de Souza

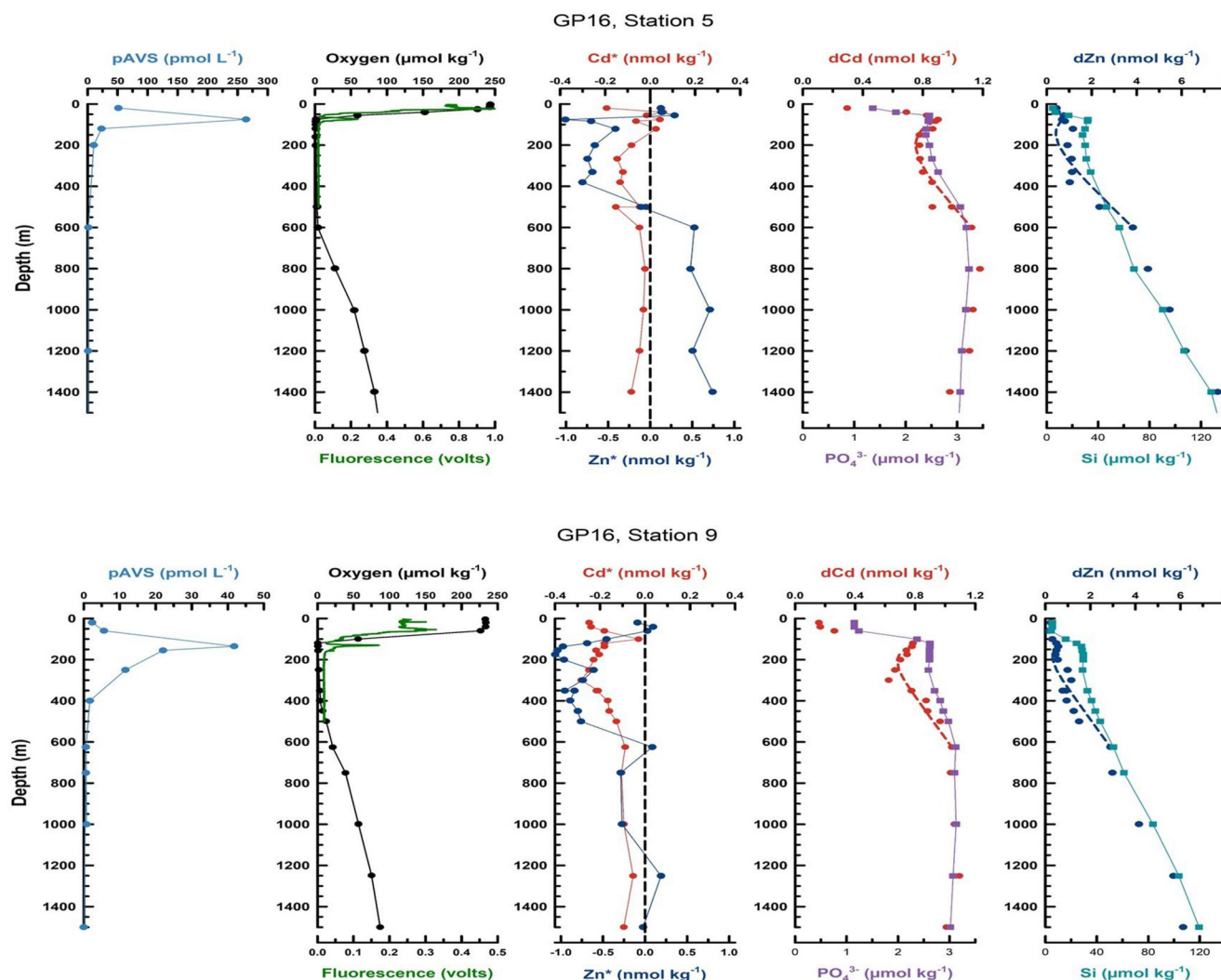


Figure 5. Vertical profiles of particulate acid-volatile sulfide (pAVS), dissolved oxygen, fluorescence, derived Cd*, derived Zn*, dissolved Cd (dCd), phosphate (PO_4^{3-}), dissolved Zn (dZn), and silicate (Si) concentrations collected on the 2013 US GEOTRACES GP16 transect in the Eastern Tropical South Pacific with Station 5 (12.0°S , 89.0°W) shown on top and Station 9 (12.0°S , 78.2°W) on the bottom. pAVS data are from Ohnemus et al. (2016) and dissolved Cd and Zn data are from John et al. (2018).

et al. (2022), respectively, but here we chose to use 0.059 and 0.35 to be most comparable to existing Pacific Zn and Cd studies, applying the same deep ocean reference ratios to both Pacific study regions in this paper for consistency. To assess the propagated uncertainty of Cd* and Zn*, we used the reported 1SD uncertainties in PO_4^{3-} ($\pm 0.02 \mu\text{mol kg}^{-1}$) and Si ($\pm 0.7 \mu\text{mol kg}^{-1}$) based on replicate measurements of their respective reference materials (Cutter, Casciotti, & Lam, 2018), in combination with the 1SD uncertainties of Cd ($\pm 0.01 \text{ nmol kg}^{-1}$) and Zn ($\pm 0.1 \text{ nmol kg}^{-1}$) based on their inter-laboratory reproducibility (see Sieber, Lanning, Bian, et al., 2023; Sieber, Lanning, Bunnell, et al., 2023, Supporting Information). Together, these yield a conservative estimate of the maximum propagated uncertainty (1SD) of $\pm 0.015 \text{ nmol kg}^{-1}$ for Cd* and $\pm 0.14 \text{ nmol kg}^{-1}$ for Zn* for the GP15 samples.

2.7. One-Dimensional Advection/Diffusion Modeling

Removal fluxes of dCd and dZn in subsurface waters were calculated using a simple one-dimensional advection/diffusion model originally developed for the deep sea and allowing non-conservative removal to be calculated (Craig, 1969), but later adapted to compute removal rates in the upper ocean (Cutter, 1991; Cutter, Moffett,

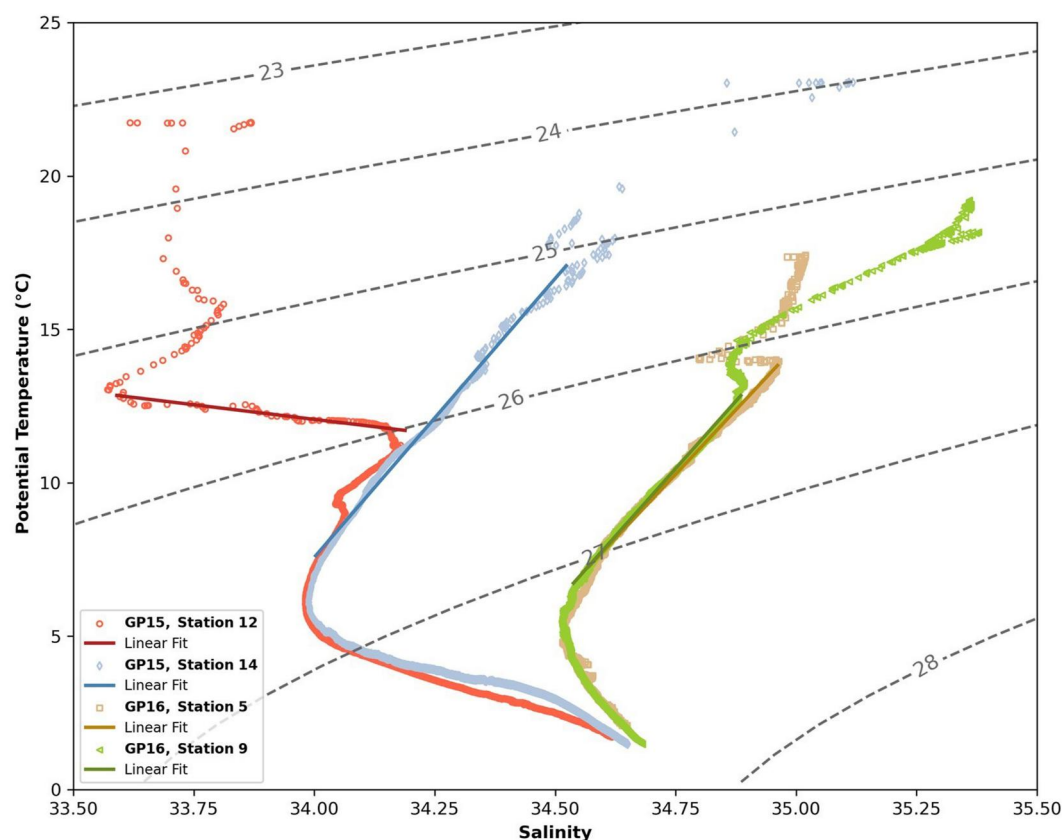


Figure 6. Temperature-salinity (T-S) diagram with density isolines of four stations from GP15 and GP16 where 1-D advection-diffusion modeling was applied. The open, red circles represent Station 12 (37°N, 152°W) from GP15, where a linear fit ($r^2 = 0.9027$) shown as a red line was applied over the modeled range (85–180 m). The open, blue diamonds represent Station 14 (32°N, 152°W) from GP15 where a linear fit ($r^2 = 0.9904$) shown as a blue line was applied over the modeled range (75–500 m). The open, brown squares represent Station 5 (12.0°S, 78.2°W) from GP16, where a linear fit ($r^2 = 0.9937$) shown as a brown line was applied over the modeled range (75–600 m). The open, green triangles represent Station 9 (12.0°S, 89°W) from GP16 where a linear fit ($r^2 = 0.9954$) shown as a green line was applied over the modeled range (135–625 m).

et al., 2018). This model assumes mixing of two end member water masses with no horizontal inputs, so it can only be applied where there is a linear T-S range (Figure 6). For this reason, it should be noted that it was only possible to apply the model to two stations in the oxic subsurface waters on GP15, and two stations in the oxycline on GP16.

In the oxygenated North Pacific for GP15, the modeling efforts used two stations. The linear T-S range for Station 12 was from 85 to 180 m and the dissolved Cd fluxes were computed over this depth range (Figure 7, top). In contrast, the linear T-S was from 75 to 500 m at Station 14 and the dCd losses were computed over this range (Figure 7, bottom). However, the large gap in the pAVS data from 150 to 500 m forced us to reduce the dissolved Cd losses to only between 75 and 150 m. For advection/diffusion calculations, ^7Be -based-vertical eddy diffusion coefficients, K_z , and upwelling rates (Moriyasu et al., 2023) at each station were used to compute a rate of production/consumption, J , that was assumed to be constant over the specified depth range. The J term was then multiplied by the depth interval to yield removal fluxes for dCd at both stations. Particulate AVS fluxes were calculated over the same depth ranges as dissolved Cd using the ^{238}U - ^{234}Th disequilibrium method (Buesseler et al., 1992) as applied to sinking particle fluxes, which combines measurements of ^{234}Th activities and pAVS concentrations on small particles (<51 μm).

Two stations from the oxycline in the ETSP for GP16 were also examined, where the linear T-S range at Station 5 ranged from 75 to 600 m and at Station 9 from 135 to 625 m. However, the dissolved Cd and Zn fluxes were only computed for the range of 75–200 m at Station 5 (Figure 8, top) and 135–200 m at Station 9 (Figure 8, bottom) to match the pAVS flux calculations since ^{234}Th fluxes were limited to the upper 200 m (Black et al., 2018). For

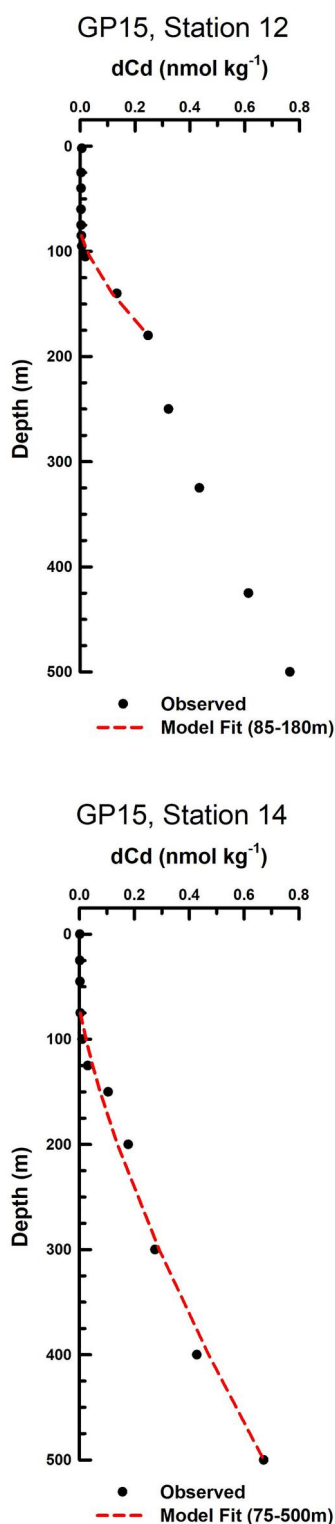


Figure 7. 1-D vertical advection/diffusion model was applied to observed dissolved Cd (dCd) at GP15 Station 12 (37.0°N, 152°W, top, $r^2 = 0.9842$) and Station 14 (32.0°N, 152.0°W, bottom, $r^2 = 0.9871$) to estimate the losses of dCd to deeper waters over the modeled range. The dashed line indicates the fit of the model to the observed dCd concentrations, which was used to calculate the rate of production/consumption of dissolved Cd.

GP16 advection/diffusion calculations, ^7Be -based-vertical eddy diffusion coefficients, K_z , and upwelling rates from Kadko (2017) at each station were used to compute a rate of production/consumption, J , that was held constant over the specified depth range as was done for the GP15 data set.

Although pAVS include CdS and ZnS precipitates, other metal sulfide precipitates are included in the pAVS fraction, such as FeS, NiS, PbS, etc. However, the precipitates PbS, CdS, and ZnS are thermodynamically favored due to lower solubility product constants and are more likely to precipitate at lower sulfide concentrations (e.g., Goates et al., 1952); they are also favored due to faster water exchange reaction kinetics (Morse & Luther, 1999). Though, due to relevant Pb, Cd, and Zn concentrations in the Pacific, it seems reasonable that CdS and ZnS precipitates are likely to make up the majority of pAVS. Therefore, this study assumes that the apparent removal is the maximum possible removal if all pAVS were bound only to Cd and Zn (for GP16) and only to Cd (for GP15; see discussion in Sections 3.1 and 3.3).

2.8. Determination of ^{234}Th

Total ^{234}Th samples were collected at all stations along the GEOTRACES GP15 (2 L samples) and GP16 (4 L samples) transects in addition to regular underway surface sampling. Total ^{234}Th analyses were done in accordance with the method developed in Buesseler et al. (2001), and further detailed in Clevenger et al. (2021). ^{234}Th was co-precipitated with Mn-oxide and collected onto a 25 mm quartz microfiber (QMA) filter and measured on Risø Laboratories anti-coincidence beta counters. A ^{230}Th yield monitor was used to determine the recovery of thorium through the chemical extraction steps. Full ^{234}Th results from GP16 are reported in Black et al. (2018). ^{238}U activities were calculated using the salinity relationship described in Owens et al. (2011):

$$^{238}\text{U}(\pm 0.047) = (0.0786 \pm 0.00446) * \text{salinity} - (0.315 \pm 0.158) \quad (3)$$

However, recent work by Xie et al. (2020) has brought into question whether the global ^{238}U -salinity relationship always holds in coastal Peruvian OMZ waters and their results indicated that using the relationship could lead to an average underestimation of ^{234}Th fluxes of 20% at locations in the vicinity of GP16 Station 5. However, in contrast to the coastal conditions observed during the austral spring-summer 2013 GP16 campaign, Xie et al. (2020) occupied the coastal waters under unique El Niño-Southern Oscillation (ENSO) and austral autumn-winter conditions in 2017 (i.e., weak alongshore winds, very low upwelling rates). The authors posited that the ENSO could be a driver for uranium mobilization from shelf sediments and it is not known whether deviations from the ^{238}U -salinity relationship could be persistent or present during the neutral La Niña years. We continue to use the ^{238}U -salinity relationship here, but we note the need for further study into ENSO-driven temporal variations in the Peruvian OMZ. The activity of ^{234}Th in the surface ocean is described by the following equation:

$$\frac{\partial^{234}\text{Th}}{\partial t} = \lambda_{\text{Th}}(^{238}\text{U} - ^{234}\text{Th}) - P_{\text{Th}_z} + V \quad (4)$$

which reflects the balance between production and loss of ^{234}Th from decay, sinking flux, and transport. ^{234}Th is the total ^{234}Th activity (dpm L^{-1}), ^{238}U is the ^{238}U activity derived from salinity, λ_{Th} is the decay constant

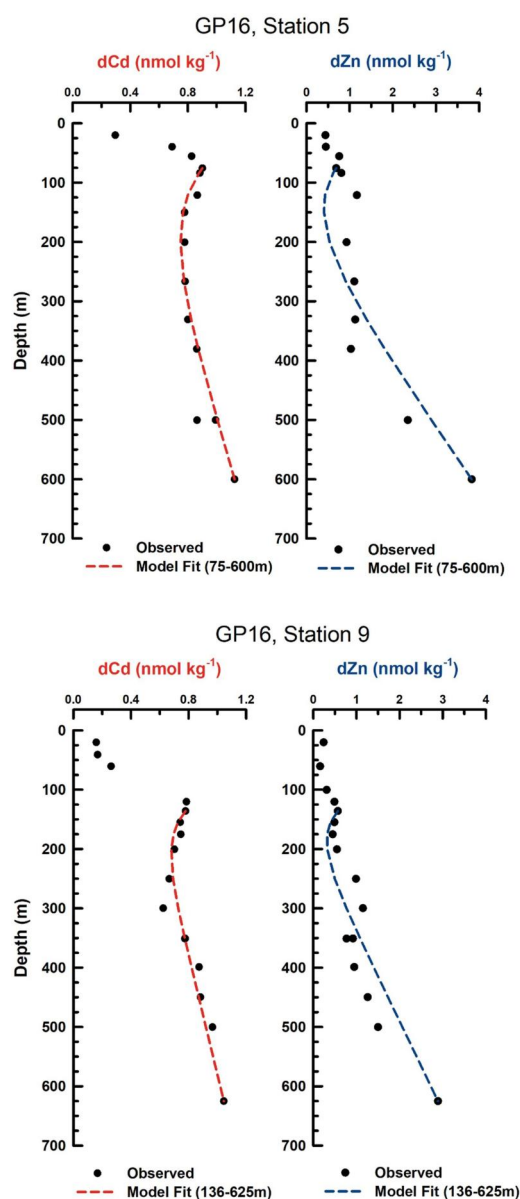


Figure 8. 1-D vertical advection/diffusion model was applied to observed dissolved Cd (dCd) and dissolved Zn (dZn) at GP16 Station 5 (12.0°S, 89.0°W, top; Cd: $r^2 = 0.7608$, Zn: $r^2 = 0.7852$) and Station 9 (12.0°S, 78.2°W, bottom; Cd: $r^2 = 0.8809$, Zn: $r^2 = 0.7280$) to estimate the losses of dCd and dZn to deeper waters over the modeled range. The dashed line indicates the fit of the model to the observed dCd and dZn concentrations, which was used to calculate the rate of production/consumption for each dissolved metal.

(0.0288 days⁻¹), P is the net removal of ²³⁴Th on sinking particles (dpm L⁻¹ d⁻¹), and V is the sum of advective and diffusive ²³⁴Th fluxes (dpm L⁻¹ d⁻¹).

The disequilibrium created between ²³⁴Th and ²³⁸U in the surface ocean occurs when thorium attaches to sinking particles. This integrated deficit can be used to determine ²³⁴Th export fluxes. In order to take the P_{Thz} term from Equation 4 and apply it to a given element or compound [E] (AVS), the following equation is needed:

$$P_{Ez} = \frac{[E]}{^{234}\text{Th}} P_{Thz} \quad (5)$$

where ^{234}Th is the activity of ²³⁴Th on sinking particles, and P_{Ez} is the particulate AVS flux at depth z . While it is often assumed that the E_{LSF}/Th_{LSF} (LSF particulates, >51 μm) measured at depth z is representative of sinking particles (reviewed in Buesseler et al. (2006)), it should be noted that the small size particle ratios have been shown to be similar to large particle ratios (Hayes et al., 2018). Therefore, demonstrating the potential of small sized fraction (SSF) pAVS contributing the same or more toward total pAVS removal compared to LSF pAVS.

3. Results and Discussion

3.1. Northeast Pacific OMZ

Janssen and co-authors (Janssen & Cullen, 2015; Janssen et al., 2014) suggested sulfide precipitation removes dCd and dZn from the OMZ depths of stations on Line P (Figure 2a) in the NE Pacific. This effect was manifested as a reported deficiency of up to 0.5 nmol kg⁻¹ of dZn and 0.1 nmol kg⁻¹ of dCd on Line P (Janssen & Cullen, 2015; Janssen et al., 2014) based on reported Zn* and Cd* anomalies. Despite US GEOTRACES GP15 stations being approximately 1,000 km west of Line P (Figure 2a), they share similarly low dissolved oxygen concentrations of <50 μmol kg⁻¹ over a 1,000 m depth range between 30°N and 55°N, with concentrations as low as 10 μmol kg⁻¹ at about 1,100 m (Figure 2b). Yet on the GP15 section, we found similar maximum apparent deficits of up to 0.1 nmol kg⁻¹ dCd but little evidence of dZn loss (Figure 3) at OMZ depths based on the calculated Zn* and Cd* anomalies. In fact, Zn* was routinely positive at the depths where we would expect to see the effects of sulfide precipitation, suggesting no significant role for sulfide-removal of Zn. This is consistent with the Zn* anomalies reported in Vance et al. (2019), which attributed the observed decoupling to differing length scales of dissolution of Zn and Si in the region, rather than in situ ZnS precipitation. Sieber, Lanning, Bian, et al. (2023) drew similar conclusions for Zn across the North Pacific, showing that Zn and Si are decoupled for several reasons, including preferential uptake and regeneration, water mass signatures, and reversible scavenging. Therefore, it is assumed that the positive anomalies seen in Zn* (Figure 3) are associated with regeneration of organic matter with an elevated Zn/Si ratio.

Below this, Zn* values return to near 0, a function of moving below the depths where regeneration of high Zn organic matter drives elevated Zn*, and not in situ Zn loss (Sieber, Lanning, Bian, et al., 2023) as ZnS precipitates.

Nonetheless, GP15 profiles exhibited slight Cd* depletions (~-0.1 nmol kg⁻¹) within the OMZ (>400 m) at several stations (featured in Figure 3), similar to Janssen et al. (2014) on Line P and Conway and John (2015b) at the SAFe Station (30°N, 140°W; approximately 1,200 km east of GP15 Station 14). Even if metal sulfide loss is limited to Cd (and not Zn) in the North Pacific OMZ, the concentrations of pAVS required to support such metal removal were not observed along our GP15 section: pAVS were <1 pmol L⁻¹

throughout the OMZ (Figures 2c and 3) and total dissolved sulfide (TDS; dissolved free and complexed sulfide) typically exhibited a near surface maximum of 50 pmol L^{-1} that decreases with depth to negligible concentrations in the OMZ (Figures 2d and 3). Overall, the observed picomolar values of TDS and pAVS are stoichiometrically too low to match the 0.1 nM deficit of dCd observed in the OMZ along GP15, and the dZn and dCd deficits previously reported on Line P (Janssen & Cullen, 2015; Janssen et al., 2014), signifying that any observed negative metal* anomalies cannot be fully explained by metal-sulfide precipitation in this region. However, one remaining question is whether particulate CdS could have sunk to deeper waters on the timescale of days to weeks (Coale & Bruland, 1985), preventing us from observing the particulate sulfides in the water column. If we assume that particulate AVS fluxes exhibited similar flux attenuation as that of carbon in the North Pacific (Buesseler et al., 2008; Martin et al., 1987), fluxes at OMZ depths (approx. 500 m) likely decreased at least 75% from the fluxes reported in the subsurface at 100 m (see Section 3.3). Under this assumption, there could have been approximately 25 pmol kg^{-1} pAVS in the OMZ (apparent deficit of dCd (0.1 nmol kg^{-1}) \times flux estimate at 500 m (25%)) at Stations 12 and 14 on GP15. This 25 pmol kg^{-1} value is still 4 times too low compared to the maximum 0.1 nmol kg^{-1} dissolved Cd deficits to explain the apparent dissolved metal deficits in the GP15 data set. Therefore, it is probable that sulfide precipitation only serves as a secondary mechanism that contributes to a portion of the dissolved Cd deficit observed in the NE Pacific OMZ, rather than the whole.

While the data examined here represent the OMZ of the NE Pacific, it should be noted that the OMZ of GP15 is deeper than the OMZ on Line P (Janssen & Cullen, 2015; Janssen et al., 2014). Station 6 (52°N , 152°W) from GP15 exhibits an oxygen depth profile (Figure 2b) more similar to Line P Stations P20 and P26 (Figure 2a). Though limited, the observed pAVS values reported in the Station 6 OMZ are also too small ($0.52 \pm 0.49 \text{ pmol pAVS L}^{-1}$, $n = 4$) to explain the apparent dissolved Cd deficits observed on Line P and GP15, even when allowing for losses by particle sinking. These data suggest that, at least in the North Pacific along GP15, dissimilatory sulfate reduction in the OMZ does not produce sufficient sulfide to fully explain the observed dCd deficits.

Instead of sulfide precipitation, recent studies invoke a circulation artifact where the apparent dissolved metal deficits observed in N. Pacific OMZs are likely a preformed signal from the Southern Ocean (de Souza et al., 2022; Middag et al., 2018, 2019; Sieber et al., 2019; Xie, Galer, et al., 2019). In this respect, Roshan and DeVries (2021) found that low-latitude oceans have lower Cd:PO₄³⁻ export ratios relative to the Southern Ocean, which acts to deplete Cd relative to phosphate in the low-latitude thermoclines. Similarly, Liu et al. (2022) also found that up to 0.5 nmol kg^{-1} Cd depletion is due to change in surface Cd:PO₄³⁻ export ratios between samples within and outside the Angola Basin OMZ instead of Cd-sulfide precipitation. More recently, Sieber, Lanning, Bunnell, et al. (2023) have argued that regeneration throughout the Pacific with a lower Cd:PO₄³⁻ than the global mean may explain apparent negative Cd* signals in this region, as such signals are not limited to low oxygen waters but rather span the whole eastern North Pacific, coinciding with the PO₄³⁻ maximum. While these studies do not rule out the precipitation of CdS and ZnS occurring in low oxygen regions, they imply that the formation of sulfide precipitates is unlikely to be the primary controlling mechanism for apparent dissolved Cd and Zn deficits observed within the NE Pacific OMZ. However, it is worth noting that the focus of this study is on small particles ($<51 \mu\text{m}$) and cannot definitively speak to the accumulation of CdS within anoxic microenvironments of large ($>51 \mu\text{m}$) sinking particles within hypoxic layers (Bianchi et al., 2018; Janssen & Cullen, 2015).

3.2. Eastern Tropical South Pacific OMZ

Comparison to a more intense OMZ, like that in the ETSP, can provide further insights into the metal-sulfide precipitation mechanism in different ocean regions. The coastal waters off Peru with high rates of productivity and particle export due to upwelling (Chavez et al., 2008) host an intense OMZ. Unlike the North Pacific OMZ, the oxygen concentrations in the ETSP reach low oxygen concentrations ($<50 \mu\text{mol kg}^{-1}$) at very shallow depths (Figure 4b). Previous studies (Xie, Rehkämper, et al., 2019) observed a decoupling between Cd and phosphate within oxygen-deficit waters, but John et al. (2018) found no evidence of large-scale Cd* depletion in the ETSP OMZ where oxygen has much lower concentrations than the other OMZs mentioned above and thus more dissimilatory sulfate reduction and metal sulfide formation might be expected (Janssen et al., 2019; John et al., 2018; Ohnemus et al., 2016). Particulate AVS data in the ETSP OMZ have been examined previously by Ohnemus et al. (2016) who concluded that the $\leq 1:1$ mol:mol ratio of Cd-to-AVS particles in the OMZ was not

Table 1

Removal Rates of Dissolved Cd and Dissolved Zn (If Apparent Deficits in Cd and Zn* Were Found) at Stations 12 and 14 on GP15, and Stations 5 and 9 on GP16*

Cruise	Station	Lat. (°N)	Long. (°W)	Depth range (m)	Cd J term (nmol L ⁻¹ d ⁻¹)	Cd flux (nmol m ⁻² d ⁻¹)	Zn J term (nmol L ⁻¹ d ⁻¹)	Zn flux (nmol m ⁻² d ⁻¹)	Measured SSF pAVS flux (nmol m ⁻² d ⁻¹)	Estimated LSF pAVS flux (nmol m ⁻² d ⁻¹)
GP15	12	37.0	152.0	85–180	$-1.4 \pm 0.4 \times 10^{-4}$	13 ± 4			4	1.7
GP15	14	32.0	152.0	75–150	$-2.5 \pm 0.2 \times 10^{-5}$	2 ± 0.2			4.5	3.4
GP16	5	-12.0	78.2	75–200	$-4.9 \pm 0.4 \times 10^{-4}$	61 ± 5	$-3.8 \pm 0.4 \times 10^{-3}$	475 ± 50	1268	609
GP16	9	-12.0	89.0	135–200	$-6.3 \pm 0.3 \times 10^{-4}$	41 ± 2	$-4.2 \pm 0.3 \times 10^{-3}$	273 ± 20	49	1.6

Note. Removal rates of particulate acid-volatile sulfide (pAVS) are reported for those four stations. It should be noted that for GP15 and GP16, only SSF pAVS was measured, and thus, those values alone are conservative estimates as they do not factor in the sinking, large particles (unmeasured). LSF pAVS fluxes were estimated using particulate Cd (LSF and SSF obtained from P. Lam) alongside LSF ²³⁴Th activities.

enough evidence to support CdS precipitation as a means to enrich Cd in sinking particles. Instead, they hypothesized (Ohnemus et al., 2016) that heterotrophs within OMZs may exhibit uniquely high Cd and Zn demands that drive metal removal from the dissolved phase relative to nutrients. Despite this prior evaluation, the US GEOTRACES GP16 section in the ETSP (Figure 4a) provides an opportunity to re-examine the pAVS data (Ohnemus et al., 2016) paired with published data for dCd and dZn (John et al., 2018) and particle flux rates using ²³⁴Th-based sinking rates (Black et al., 2018) above and within an OMZ. These thorium data were not yet available for the Ohnemus et al. (2016) study.

Apparent dCd and dZn deficits were calculated as part of our reanalysis of GP16 results using the same ‘star’ convention (see Section 2.6) to compare to the NE Pacific. However, we need to consider equatorial Antarctic Intermediate Water (eqAAIW) that supplies Cd and Zn to these waters, which carries preformed southern-sourced Cd* ($-0.1 \text{ nmol kg}^{-1}$ (Sieber et al., 2019)) and Zn* signals ($-0.5 \text{ nmol kg}^{-1}$ (John et al., 2018)). After factoring in the preformed eqAAIW signal, GP16 stations exhibit apparent local deficits of dCd up to 0.2 nmol kg^{-1} and 0.7 nmol kg^{-1} dZn in the OMZ at Stations 5 and 9 according to Cd* and Zn* values (Figure 5). In contrast to the North Pacific OMZ, shallow OMZ depths in the ETSP display large peaks in pAVS (Ohnemus et al., 2016) (Figures 4c and 5), with Station 5 showing a pAVS maximum of 264 pmol L^{-1} at the base of the oxycline (Figure 5, top). Station 9 also exhibited a pAVS maximum at the base of the oxycline, although it only reached 42 pmol L^{-1} pAVS (Figure 5, bottom).

To quantify the losses of dCd and dZn on the GP16 transect and compare them to pAVS fluxes, removal fluxes of dCd and dZn were calculated using the simple one-dimensional advection/diffusion model covered in Section 2.7 and used by Cutter, Moffett, et al. (2018) for the same stations on GP16. The calculated Zn and Cd removal rates (Table 1) were more than an order of magnitude higher in the ETSP (GP16) than in the NE Pacific (GP15). To compare these dissolved metal losses, particulate AVS fluxes were calculated over the same depth ranges using ²³⁸U-²³⁴Th disequilibrium (see Section 2.8) as applied to sinking particle fluxes. The more coastal Station 5 saw a pAVS net removal rate of $1,268 \text{ nmol S m}^{-2} \text{ d}^{-1}$ between 75 and 200 m in the SSF, while Station 9 had an SSF pAVS net removal rate of $49 \text{ nmol S m}^{-2} \text{ d}^{-1}$ (Table 1) between 135 and 200 m. As such, Station 5 had more than enough pAVS flux to account for the apparent removal of both dCd and dZn in the shallow upper OMZ, while at Station 9 it could account for 16% of the apparent dissolved removal of dCd and dZn (Table 1) as small CdS and ZnS precipitates. However, it is important to note that these estimates of dCd and dZn removal as pAVS only account for the measured SSF that is being fluxed to deeper waters. Therefore, our reported SSF pAVS flux is a conservative minimum since they do not include the more commonly considered sinking (e.g., Lam et al., 2018; Lee et al., 2018) LSF particles (unmeasured). Considering that pAVS is likely primarily composed of CdS (and possibly ZnS) precipitates, it is assumed that the particle distribution of pAVS resembles the pattern of distribution seen for particulate Cd (Lee et al., 2018). To address this caveat, LSF pAVS fluxes were estimated at both stations using particulate Cd concentrations (LSF and SSF; obtained from P. Lam) alongside the LSF ²³⁴Th activities. Although all of the dCd and dZn losses observed at Station 5 could be explained by the SSF pAVS, removal at Station 9 was more limited. If LSF pAVS removal is considered, dCd and dZn removal via precipitation with sulfide potentially removes an additional $1.6 \text{ nmol S m}^{-2} \text{ d}^{-1}$ at Station 9 (Table 1), accounting for 1% increase in the estimated loss of dissolved Cd and Zn in the oxycline. These estimates suggest that the measured SSF

pAVS likely makes up a larger proportion of the total pAVS (SSF + LSF) flux and thus serves a larger role in the removal of dCd and dZn as metal-sulfide precipitates in the shallow, upper OMZ waters, instead of the unmeasured LSF pAVS.

These GP16 results confirm that metal removal via precipitation with sulfide is possible, but it is important to point out that the OMZ off Peru is unique. While dissimilatory sulfate reduction has been documented in OMZ waters (Callbeck et al., 2021; Canfield et al., 2010; Schlosser et al., 2018), the pAVS maxima coincide with the secondary fluorescence maxima (Figure 5) (Ohnemus et al., 2016) where photosynthetic bacteria are present (Goericke et al., 2000; Lavin et al., 2010). Thus, it is likely that some fraction of TDS (not measured on GP16) and pAVS are associated with assimilatory sulfate reduction during photosynthesis at these depths (Walsh et al., 1994). As a result, both assimilatory sulfate reduction (Ohnemus et al., 2016; Walsh et al., 1994) and dissimilatory sulfate reduction (Canfield et al., 2010) may contribute to the observed dCd and dZn losses in the ETSP, potentially explaining the contrasting patterns observed in different OMZs.

3.3. Northeast Pacific Oxidic Subsurface

In contrast to the low concentrations at OMZ depths in the Northeast Pacific, both pAVS and TDS concentrations are highest in the upper 200 m of the water column (Figures 2 and 3), where oxygen is abundant ($>200 \mu\text{mol kg}^{-1}$). Unlike GP16, no evidence of dZn loss was found in the Northeast Pacific on GP15 as indicated by Zn* (Figure 3). However, apparent dCd deficits up to 0.1 nmol kg^{-1} were reported at Stations 12, 14, and 16, and up to $0.15 \text{ nmol kg}^{-1}$ at Station 10 from GP15 (Figure 3) in the oxygenated subsurface. In these same waters are where Sieber, Lanning, Bunnell, et al. (2023) reported a heavier dissolved isotope signal ($\delta^{114}\text{Cd}$) which would be consistent with CdS precipitation that preferentially incorporates light Cd isotopes into the particulate phase. Significantly, this is also where pAVS reach maxima that coincide with the local Cd* minima in the GP15 profiles (Figure 3), and therefore sinking pAVS could lead to removal of Cd in oxic waters.

To quantify the losses of dCd on the GP15 transect and compare them to pAVS fluxes, we used the same computations as those used for the GP16 data set (Sections 2.7 and 3.2). The removal rate of dCd at Station 12 (Cd flux is $13 \pm 4 \text{ nmol m}^{-2} \text{ d}^{-1}$; Table 1) was 6.5 times larger than those calculated at Station 14 (Cd flux is $2 \pm 0.2 \text{ nmol m}^{-2} \text{ d}^{-1}$; Table 1). These dissolved Cd removals could be due to sulfide precipitation or adsorptive loss. Similar to GP16, ^{234}Th data (Black et al., 2018) were used to calculate pAVS removal fluxes on GP15, where Station 12 saw an SSF pAVS net removal rate of $4 \text{ nmol S m}^{-2} \text{ d}^{-1}$ between 85 and 180 m, while Station 14 had an SSF pAVS net removal rate of $4.5 \text{ nmol S m}^{-2} \text{ d}^{-1}$ (Table 1) between 75 and 150 m. Therefore, CdS precipitation as small pAVS could potentially explain up to 31% of subsurface dCd losses at Station 12 and all dCd losses at Station 14 (Table 1), assuming that all SSF pAVS were bound only to Cd. However, it is likely that some fraction of pAVS is bound to other metals such as Zn and Pb (see Section 2.7). These other metal-sulfide precipitates might account for a portion of the excess SSF pAVS removal calculated at Station 14 ($2.5 \text{ nmol S m}^{-2} \text{ d}^{-1}$ in excess) compared to dCd removal. Like GP16, these removal estimates are likely underestimates of the total possible removal as pAVS since only the SSF pAVS were measured on GP15. Considering that pAVS is likely to be predominately composed of CdS precipitates, it is presumed that most of pAVS resides in the SSF rather than the LSF. After estimating LSF pAVS fluxes using particulate Cd concentrations (LSF and SSF; obtained from P. Lam) and LSF ^{234}Th activities, results suggest that the contribution of LSF pAVS to the apparent removal of dCd in the oxic subsurface is less than that of the measured SSF pAVS (Table 1). While all dCd losses at Station 14 can be explained by small CdS particles, large sinking particles might also contribute to the removal of dCd observed at Station 12. Dissolved Cd removal via precipitation as large CdS potentially removes an additional $1.7 \text{ nmol S m}^{-2} \text{ d}^{-1}$ at Station 12 (Table 1). Therefore, small and large pAVS could account for up to 44% of the estimated dCd losses observed in the oxic upper water column at Station 12.

These fluxes suggest that CdS formation in near surface waters are more likely to explain the dissolved Cd deficits in the NE Pacific rather than in the OMZ where it was originally proposed (Janssen & Cullen, 2015; Janssen et al., 2014). Markedly, in these near surface waters is where we generally see the largest dissolved Cd deficits as indicated by Cd*, alongside pAVS and fluorescence maxima—similar to GP16 results at Stations 5 and 9. In these oxic surface waters, sulfide is produced from assimilatory sulfate reduction (Walsh et al., 1994) instead of the dissimilatory sulfate reduction proposed for OMZs (Canfield et al., 2010).

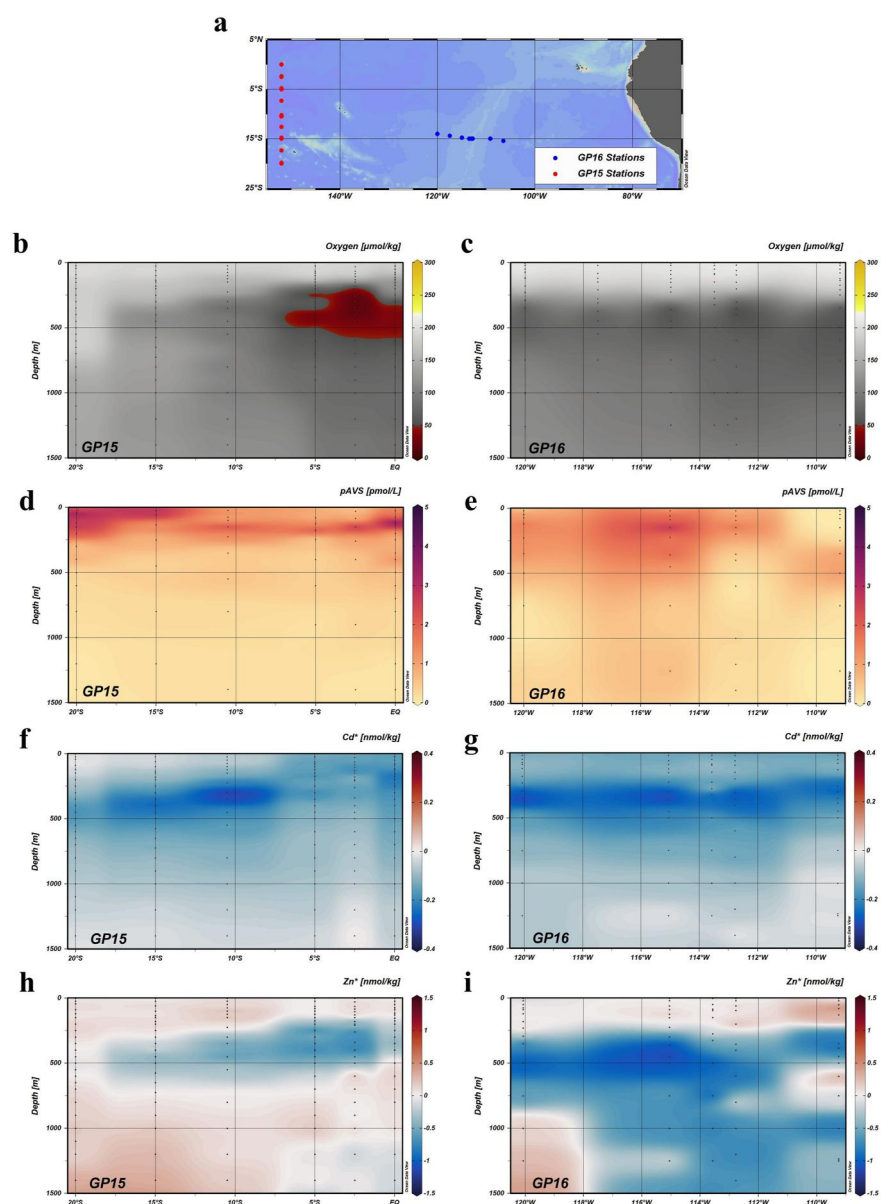


Figure 9. Sampling locations in the oxygenated, open Pacific Ocean (panel a) where blue dots are stations west of 109°W on the 2013 US GEOTRACES GP16 and red dots are sampling locations south of the equator on the 2018 US GEOTRACES GP15. Contoured transect profiles of dissolved oxygen (panel b), particulate acid volatile sulfide (pAVS; panel d), derived Cd^* (panel f), and derived Zn^* (panel h) concentrations from those GP15 sampling locations are shown for the upper 1,500 m with original data points shown as black dots. Contoured transect profiles of dissolved oxygen (panel c), pAVS (panel e), derived Cd^* (panel g), and derived Zn^* (panel i) concentrations from those GP16 sampling locations are shown for the upper 1,500 m with original data points shown as black dots. Zn^* and Cd^* profiles for GP15 were reported by Sieber, Lanning, Bian, et al. (2023) and Sieber, Lanning, Bunnell, et al. (2023), respectively. A subset of those data were replotted in panels (f) and (h). Zn^* and Cd^* profiles for GP16 (panels g and i) were plotted from data reported by John et al. (2018).

4. Conclusions

Overall, we combined sulfide and dissolved metal measurements to test the hypothesis of Janssen and co-authors (Janssen & Cullen, 2015; Janssen et al., 2014) that dissimilatory sulfate reduction within anoxic microenvironments of sinking organic particles facilitates dCd and dZn loss via metal-sulfide precipitation in OMZs. Within the NE Pacific OMZ, picomolar pAVS and TDS values were too low to account for the apparent nanomolar deficits in dCd. Thus, CdS precipitation cannot be the primary mechanism responsible for the apparent deficits of

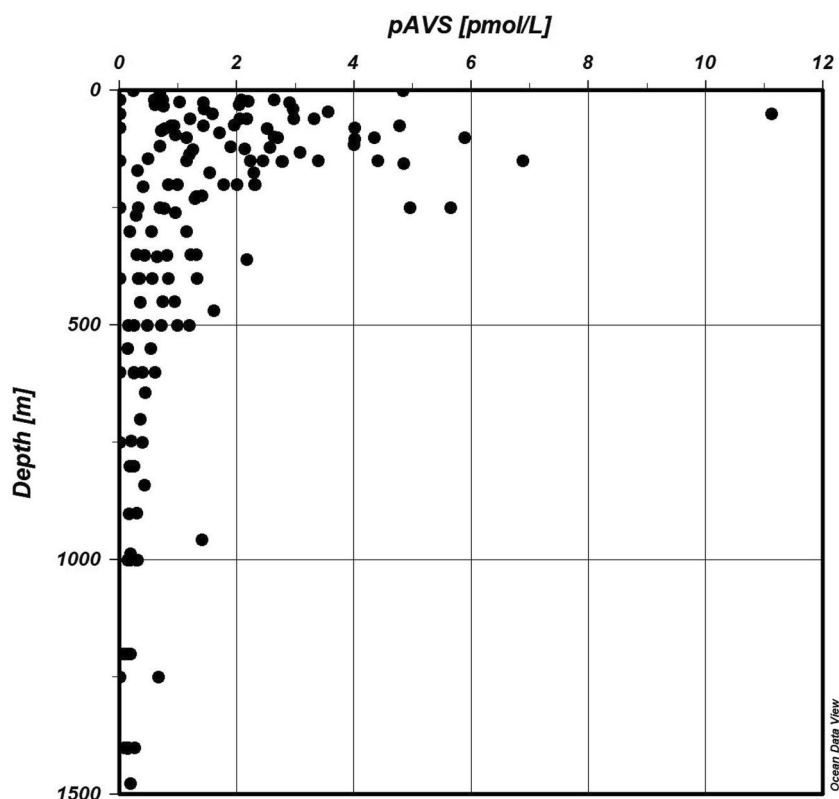


Figure 10. Particulate acid volatile sulfide (pAVS) data from the upper 1,500 m of the oxygenated Pacific Ocean on GP15 and GP16 (from all stations shown in panel a of Figure 9), three stations (5°S , 138.3°W ; 0°N , 140°W ; 15°N , 152.5°W) occupied in the central equatorial Pacific Ocean during August 1991, and two profiles from the BATS (31.8°N , 64.2°W) station in the North Atlantic Ocean during April 1989 and March 1995 where concentrations occasionally exceed 5 pmol L^{-1} . The pAVS data from BATS in April 1989 were replotted from data reported in Cutter and Radford-Knoery (1991). Particulate AVS data from GP15 and GP16 represent only the small sized fraction ($0.8\text{--}51 \text{ }\mu\text{m}$). pAVS data from BATS (1989 and 1995) and from the central equatorial Pacific in 1991 were obtained using a $0.4 \text{ }\mu\text{m}$ filter and thus included both the small and large size particles as there was no prefilter.

dCd in the NE Pacific OMZ, as pointed out by others (de Souza et al., 2022; Janssen et al., 2019; Middag et al., 2018, 2019; Sieber et al., 2019; Xie, Galer, et al., 2019). Instead, the decoupling of Cd from PO_4^{3-} (and Zn from Si) are likely a consequence of the physical circulation, variable stoichiometry of biological uptake, and/or different regeneration length scales of micro- and macronutrients (de Souza et al., 2022; Middag et al., 2018, 2019; Sieber et al., 2019; Sieber, Lanning, Bian, et al., 2023; Sieber, Lanning, Bunnell, et al., 2023; Vance et al., 2019; Weber et al., 2018; Xie, Galer, et al., 2019).

We speculate that the observed metal deficits in the more intense OMZ in the ETSP can be explained by a combination of both assimilatory and dissimilatory sulfate reduction producing sulfide (Figure 1) due to the shoaling of the oxycline into shallower waters and the euphotic zone. Together, Stations 5 and 9 from GP16 support the hypothesis that metal-sulfide precipitation can account for at least a portion of dCd and dZn metal loss from the water column, not only within OMZs but also from shallow oxygenated ocean layers. Even so, we cannot speculate on whether this unique combination of assimilatory and dissimilatory processes is present in other ocean OMZs.

However, the GP15 data set and associated flux calculations support a revised metal-sulfide removal process that occurs in near surface waters where the greatest apparent dissolved Cd deficits appear along with pAVS and fluorescence maxima (Figure 3 and Table 1). The areal extent of this revised hypothesis is supported by the dCd anomalies observed in oxygenated water globally (Baars et al., 2014; Conway & John, 2015a, 2015b; de Souza et al., 2022; Janssen et al., 2014; Sieber, Lanning, Bunnell, et al., 2023) in the upper 300 m. Further support is found in the oxygenated central Pacific (GP15 and GP16) where the largest dissolved Cd and Zn deficits typically

occur in the upper 500 m where pAVS concentrations are also greatest (Figure 9). Although limited, additional sulfide data from the oxygenated N. Atlantic (Cutter & Radford-Knoery, 1991) and central Pacific (Radford-Knoery, 1993) display elevated total pAVS (<0.4 μm) concentrations in the upper 200 m (Figure 10), suggesting that Cd precipitation as sulfides might play a global role in the removal of dissolved Cd in the oxic subsurface. We suggest that in this revised removal scenario, metals such as Cd (and perhaps Zn) are partly removed from the water column by phytoplankton production of free sulfide (Figure 1) via assimilatory sulfate reduction as a by-product of photosynthesis (Walsh et al., 1994). Taken together, our results suggest that the removal of dCd and dZn in low oxygen environments via precipitation with sulfides likely varies regionally. In contrast, the negative anomalies in dCd, and the pAVS abundance in the oxic upper 200 m may be an important sink in upper ocean removal on a global scale and support a revised process for metal-sulfide precipitation in surface waters.

Conflict of Interest

The authors declare no conflicts of interest relevant to this study.

Data Availability Statement

Data used in this manuscript can be accessed from the Biological & Chemical Oceanography Data Management Office (BCO-DMO). GP16 particulate sulfide (<https://www.bco-dmo.org/dataset/646143>), dissolved Zn and Cd (<https://www.bco-dmo.org/dataset/643809>), thorium-234 (<https://www.bco-dmo.org/dataset/643316> and <https://www.bco-dmo.org/dataset/643213>), and beryllium-7 (<https://www.bco-dmo.org/dataset/665158>). GP15 total dissolved (<https://www.bco-dmo.org/dataset/873908> and <https://www.bco-dmo.org/dataset/873927>) and particulate sulfide (<https://www.bco-dmo.org/dataset/873765> and <https://www.bco-dmo.org/dataset/873792>), dissolved Zn and Cd measured by USF (<https://www.bco-dmo.org/dataset/883862>), thorium-234 (<https://www.bco-dmo.org/dataset/812511>), and beryllium-7 (<https://www.bco-dmo.org/dataset/781794>). Dissolved Zn and Cd data measured at TAMU will be available on BCO-DMO in the future but was not yet at the time of publication. Ocean Data View (Schlitzer, 2023) was used to produce Figures 2, 4, 9 and 10.

References

- Baars, O., Abouchami, W., Galer, S. J. G., Boye, M., & Croot, P. L. (2014). Dissolved cadmium in the Southern Ocean: Distribution, speciation, and relation to phosphate. *Limnology & Oceanography*, 59(2), 385–399. <https://doi.org/10.4319/lo.2014.59.2.0385>
- Bianchi, D., Weber, T. S., Kiko, R., & Deutsch, C. (2018). Global niche of marine anaerobic metabolisms expanded by particle microenvironments. *Nature Geoscience*, 11(4), 263–268. Article 4. <https://doi.org/10.1038/s41561-018-0081-0>
- Bishop, J. K. B., Lam, P. J., & Wood, T. J. (2012). Getting good particles: Accurate sampling of particles by large volume in-situ filtration. *Limnology and Oceanography: Methods*, 10(9), 681–710. <https://doi.org/10.4319/lom.2012.10.681>
- Black, E. E., Buesseler, K. O., Pike, S. M., & Lam, P. J. (2018). 234Th as a tracer of particulate export and remineralization in the southeastern tropical Pacific. *Marine Chemistry*, 201, 35–50. <https://doi.org/10.1016/j.marchem.2017.06.009>
- Black, E. E., Lam, P. J., Lee, J.-M., & Buesseler, K. O. (2019). Insights from the 238U-234Th method into the coupling of biological export and the cycling of cadmium, cobalt, and manganese in the southeast Pacific Ocean. *Global Biogeochemical Cycles*, 33(1), 15–36. <https://doi.org/10.1029/2018GB005985>
- Boyle, E. A., Sclater, F., & Edmond, J. M. (1976). On the marine geochemistry of cadmium. *Nature*, 263(5572), 42–44. <https://doi.org/10.1038/263042a0>
- Bruland, K. W., Knauer, G. A., & Martin, J. H. (1978). Zinc in north-east Pacific water. *Nature*, 271(5647), 741–743. <https://doi.org/10.1038/271741a0>
- Bruland, K. W., & Lohan, M. C. (2006). Controls of trace metals in seawater. In *Treatise on geochemistry* (1st ed., Vol. 6, pp. 23–47). Elsevier.
- Buesseler, K. O., Bacon, M. P., Kirk Cochran, J., & Livingston, H. D. (1992). Carbon and nitrogen export during the JGOFS North Atlantic bloom experiment estimated from 234Th: 238U disequilibria. *Deep-Sea Research, Part A: Oceanographic Research Papers*, 39(7), 1115–1137. [https://doi.org/10.1016/0198-0149\(92\)90060-7](https://doi.org/10.1016/0198-0149(92)90060-7)
- Buesseler, K. O., Benitez-Nelson, C., Rutgers van der Loeff, M., Andrews, J., Ball, L., Crossin, G., & Charette, M. A. (2001). An intercomparison of small- and large-volume techniques for thorium-234 in seawater. *Marine Chemistry*, 74(1), 15–28. [https://doi.org/10.1016/S0304-4203\(00\)00092-X](https://doi.org/10.1016/S0304-4203(00)00092-X)
- Buesseler, K. O., Benitez-Nelson, C. R., Moran, S. B., Burd, A., Charette, M., Cochran, J. K., et al. (2006). An assessment of particulate organic carbon to thorium-234 ratios in the ocean and their impact on the application of 234Th as a POC flux proxy. *Marine Chemistry*, 100(3), 213–233. <https://doi.org/10.1016/j.marchem.2005.10.013>
- Buesseler, K. O., Trull, T. W., Steinberg, D. K., Silver, M. W., Siegel, D. A., Saitoh, S.-I., et al. (2008). VERTIGO (VERTical Transport in the Global Ocean): A study of particle sources and flux attenuation in the North Pacific. *Deep Sea Research Part II: Topical Studies in Oceanography*, 55(14), 1522–1539. <https://doi.org/10.1016/j.dsr2.2008.04.024>
- Callbeck, C. M., Canfield, D. E., Kuypers, M. M. M., Yilmaz, P., Lavik, G., Thamdrup, B., et al. (2021). Sulfur cycling in oceanic oxygen minimum zones. *Limnology & Oceanography*, 66(6), 2360–2392. <https://doi.org/10.1002/lno.11759>
- Canfield, D. E., Stewart, F. J., Thamdrup, B., Brabandere, L. D., Dalsgaard, T., Delong, E. F., et al. (2010). A cryptic sulfur cycle in oxygen-minimum-zone waters off the Chilean coast. *Science*, 330(6009), 1375–1378. <https://doi.org/10.1126/science.1196889>
- Chavez, F. P., Bertrand, A., Guevara-Carrasco, R., Soler, P., & Csirke, J. (2008). The northern Humboldt Current System: Brief history, present status and a view towards the future. *Progress in Oceanography*, 79(2), 95–105. <https://doi.org/10.1016/j.pocean.2008.10.012>

Acknowledgments

We thank the captain and crew of R/V *Roger Revelle*, and the dissolved and particulate sampling teams of US GEOTRACES Pacific Meridional Transect. US GEOTRACES GP15 work was funded by National Science Foundation Grants (OCE-1737342 to Greg Cutter, OCE-1735445 to Ken Buesseler, OCE-1737136 to Tim Conway, OCE-1737167 to Jessica Fitzsimmons, and GRFP-1746932 to Nathan Lanning). US GEOTRACES GP16 work was funded by National Science Foundation Grants (OCE-1235328 to Greg Cutter, OCE-1232669 to Ken Buesseler and Matthew Charette, and OCE-1649439 to Seth John).

- Clevenger, S. J., Benitez-Nelson, C. R., Drysdale, J., Pike, S., Puigcorb , V., & Buesseler, K. O. (2021). Review of the analysis of ²³⁴Th in small volume (2–4 L) seawater samples: Improvements and recommendations. *Journal of Radioanalytical and Nuclear Chemistry*, 329(1), 1–13. <https://doi.org/10.1007/s10967-021-07772-2>
- Coale, K. H., & Bruland, K. W. (1985). ²³⁴Th:²³⁸U disequilibria within the California Current. *Limnology & Oceanography*, 30(1), 22–33. <https://doi.org/10.4319/lm.1985.30.1.0022>
- Conway, T. M., & John, S. G. (2014). The biogeochemical cycling of zinc and zinc isotopes in the North Atlantic Ocean. *Global Biogeochemical Cycles*, 28(10), 1111–1128. <https://doi.org/10.1002/2014GB004862>
- Conway, T. M., & John, S. G. (2015a). Biogeochemical cycling of cadmium isotopes along a high-resolution section through the North Atlantic Ocean. *Geochimica et Cosmochimica Acta*, 148, 269–283. <https://doi.org/10.1016/j.gca.2014.09.032>
- Conway, T. M., & John, S. G. (2015b). The cycling of iron, zinc and cadmium in the North East Pacific Ocean – Insights from stable isotopes. *Geochimica et Cosmochimica Acta*, 164, 262–283. <https://doi.org/10.1016/j.gca.2015.05.023>
- Conway, T. M., Rosenberg, A. D., Adkins, J. F., & John, S. G. (2013). A new method for precise determination of iron, zinc and cadmium stable isotope ratios in seawater by double-spike mass spectrometry. *Analytica Chimica Acta*, 793, 44–52. <https://doi.org/10.1016/j.aca.2013.07.025>
- Craig, H. (1969). Abyssal carbon and radiocarbon in the Pacific. *Journal of Geophysical Research*, 74(23), 5491–5506. <https://doi.org/10.1029/JC074i023p05491>
- Cutter, G. A. (1991). Dissolved arsenic and antimony in the black sea. *Deep-Sea Research, Part A: Oceanographic Research Papers*, 38, S825–S843. [https://doi.org/10.1016/S0198-0149\(10\)80011-1](https://doi.org/10.1016/S0198-0149(10)80011-1)
- Cutter, G. A., & Bruland, K. W. (2012). Rapid and noncontaminating sampling system for trace elements in global ocean surveys. *Limnology and Oceanography: Methods*, 10(6), 425–436. <https://doi.org/10.4319/lom.2012.10.425>
- Cutter, G. A., Casciotti, K., Croot, P., Geibert, W., Heimb rger, L.-E., Lohan, M., et al. (2017). Sampling and sample-handling protocols for GEOTRACES cruises. Version 3, August 2017. [Report]. GEOTRACES International Project Office. <https://repository.oceanbestpractices.org/handle/11329/409>
- Cutter, G. A., Casciotti, K., & Lam, P. J. (2018). US GEOTRACES Pacific meridional transect—GP15 cruise report. Retrieved from https://datadocs.bco-dmo.org/docs/geotraces/GEOTRACES_PMT/casciotti/data_docs/GP15_Cruise_Report_with_ODF_Report.pdf
- Cutter, G. A., & Kluckhohn, R. S. (1999). The cycling of particulate carbon, nitrogen, sulfur, and sulfur species (iron monosulfide, greigite, pyrite, and organic sulfur) in the water columns of Framvaren Fjord and the Black Sea. *Marine Chemistry*, 67(3), 149–160. [https://doi.org/10.1016/S0304-4203\(99\)00056-0](https://doi.org/10.1016/S0304-4203(99)00056-0)
- Cutter, G. A., Moffett, J., Nielsd ttir, M. C., & Sanial, V. (2018). Multiple oxidation state trace elements in suboxic waters off Peru: In situ redox processes and advective/diffusive horizontal transport. *Marine Chemistry*, 201, 77–89. <https://doi.org/10.1016/j.marchem.2018.01.003>
- Cutter, G. A., & Radford-Knoery, J. (1991). Determination of carbon, nitrogen, sulfur, and inorganic sulfur species in marine particles. In *Marine particles: Analysis and characterization* (pp. 57–63). American Geophysical Union (AGU). <https://doi.org/10.1029/GM063p0057>
- de Souza, G. F., Vance, D., Sieber, M., Conway, T. M., & Little, S. H. (2022). Re-assessing the influence of particle-hosted sulphide precipitation on the marine cadmium cycle. *Geochimica et Cosmochimica Acta*, 322, 274–296. <https://doi.org/10.1016/j.gca.2022.02.009>
- Elliott, S., Lu, E., & Rowland, F. S. (1987). Carbonyl sulfide hydrolysis as a source of hydrogen sulfide in open ocean seawater. *Geophysical Research Letters*, 14(2), 131–134. <https://doi.org/10.1029/GL014i002p00131>
- Goates, J. R., Gordon, M. B., & Faux, N. (1952). Calculated values for the solubility product constants of the metallic sulfides. *Journal of the American Chemical Society*, 74(3), 835–836. <https://doi.org/10.1021/ja01123a510>
- Goerike, R., Olson, R. J., & Shalapyonok, A. (2000). A novel niche for *Prochlorococcus* sp. in low-light suboxic environments in the Arabian Sea and the Eastern Tropical North Pacific. *Deep Sea Research Part I: Oceanographic Research Papers*, 47(7), 1183–1205. [https://doi.org/10.1016/S0967-0637\(99\)00108-9](https://doi.org/10.1016/S0967-0637(99)00108-9)
- Guinoiseau, D., Galer, S. J. G., & Abouchami, W. (2018). Effect of cadmium sulphide precipitation on the partitioning of Cd isotopes: Implications for the oceanic Cd cycle. *Earth and Planetary Science Letters*, 498, 300–308. <https://doi.org/10.1016/j.epsl.2018.06.039>
- Guinoiseau, D., Galer, S. J. G., Abouchami, W., Frank, M., Achterberg, E. P., & Haug, G. H. (2019). Importance of cadmium sulfides for biogeochemical cycling of Cd and its isotopes in oxygen deficient zones—A case study of the Angola Basin. *Global Biogeochemical Cycles*, 33(12), 1746–1763. <https://doi.org/10.1029/2019GB006323>
- Hayes, C. T., Black, E. E., Anderson, R. F., Baskaran, M., Buesseler, K. O., Charette, M. A., et al. (2018). Flux of particulate elements in the North Atlantic Ocean constrained by multiple radionuclides. *Global Biogeochemical Cycles*, 32(12), 1738–1758. <https://doi.org/10.1029/2018GB005994>
- Janssen, D. J., Abouchami, W., Galer, S. J. G., Purdon, K. B., & Cullen, J. T. (2019). Particulate cadmium stable isotopes in the subarctic northeast Pacific reveal dynamic Cd cycling and a new isotopically light Cd sink. *Earth and Planetary Science Letters*, 515, 67–78. <https://doi.org/10.1016/j.epsl.2019.03.006>
- Janssen, D. J., Conway, T. M., John, S. G., Christian, J. R., Kramer, D. I., Pedersen, T. F., & Cullen, J. T. (2014). Undocumented water column sink for cadmium in open ocean oxygen-deficient zones. *Proceedings of the National Academy of Sciences*, 111(19), 6888–6893. <https://doi.org/10.1073/pnas.1402388111>
- Janssen, D. J., & Cullen, J. T. (2015). Decoupling of zinc and silicic acid in the subarctic northeast Pacific interior. *Marine Chemistry*, 177, 124–133. <https://doi.org/10.1016/j.marchem.2015.03.014>
- Jensen, L. T., Wyatt, N. J., Landing, W. M., & Fitzsimmons, J. N. (2020). Assessment of the stability, sorption, and exchangeability of marine dissolved and colloidal metals. *Marine Chemistry*, 220, 103754. <https://doi.org/10.1016/j.marchem.2020.103754>
- Jia-Zhong, Z., & Whitfield, M. (1986). Kinetics of inorganic redox reactions in seawater: I. The reduction of iodate by bisulphide. *Marine Chemistry*, 19(2), 121–137. [https://doi.org/10.1016/0304-4203\(86\)90044-7](https://doi.org/10.1016/0304-4203(86)90044-7)
- John, S. G., Helgoe, J., & Townsend, E. (2018). Biogeochemical cycling of Zn and Cd and their stable isotopes in the eastern Tropical South Pacific. *Marine Chemistry*, 201, 256–262. <https://doi.org/10.1016/j.marchem.2017.06.001>
- Kadko, D. (2017). Upwelling and primary production during the U.S. GEOTRACES East Pacific Zonal Transect. *Global Biogeochemical Cycles*, 31(2), 218–232. <https://doi.org/10.1002/2016GB005554>
- Lam, P. J., Lee, J.-M., Heller, M. I., Mehic, S., Xiang, Y., & Bates, N. R. (2018). Size-fractionated distributions of suspended particle concentration and major phase composition from the U.S. GEOTRACES Eastern Pacific Zonal Transect (GP16). *Marine Chemistry*, 201, 90–107. <https://doi.org/10.1016/j.marchem.2017.08.013>
- Lavin, P., Gonz lez, B., Santib niz, J. F., Scanlan, D. J., & Ulloa, O. (2010). Novel lineages of *Prochlorococcus* thrive within the oxygen minimum zone of the eastern tropical South Pacific. *Environmental Microbiology Reports*, 2(6), 728–738. <https://doi.org/10.1111/j.1758-2229.2010.00167.x>
- Lee, J.-M., Heller, M. I., & Lam, P. J. (2018). Size distribution of particulate trace elements in the U.S. GEOTRACES Eastern Pacific Zonal Transect (GP16). *Marine Chemistry*, 201, 108–123. <https://doi.org/10.1016/j.marchem.2017.09.006>

- Liu, T., Krisch, S., Xie, R. C., Hopwood, M. J., Dengler, M., & Achterberg, E. P. (2022). Sediment release in the Benguela Upwelling System dominates trace metal input to the shelf and eastern South Atlantic Ocean. *Global Biogeochemical Cycles*, *36*(9), e2022GB007466. <https://doi.org/10.1029/2022GB007466>
- Martin, J. H., Knauer, G. A., Karl, D. M., & Broenkow, W. W. (1987). VERTEX: Carbon cycling in the northeast Pacific. *Deep-Sea Research, Part A: Oceanographic Research Papers*, *34*(2), 267–285. [https://doi.org/10.1016/0198-0149\(87\)90086-0](https://doi.org/10.1016/0198-0149(87)90086-0)
- Middag, R., Baar, H. J. W., & Bruland, K. W. (2019). The relationships between dissolved zinc and major nutrients phosphate and silicate along the GEOTRACES GA02 transect in the West Atlantic Ocean. *Global Biogeochemical Cycles*, *33*(1), 63–84. <https://doi.org/10.1029/2018GB006034>
- Middag, R., van Heuven, S. M. A. C., Bruland, K. W., & de Baar, H. J. W. (2018). The relationship between cadmium and phosphate in the Atlantic Ocean unravelled. *Earth and Planetary Science Letters*, *492*, 79–88. <https://doi.org/10.1016/j.epsl.2018.03.046>
- Millero, F. J., Hubinger-Fernandez, S. M., Fernandez, M., & Garnett, S. (1987). Oxidation of H₂S in seawater as a function of temperature, pH, and ionic strength. *Environmental Science & Technology*, *21*(5), 439–443. <https://doi.org/10.1021/es00159a003>
- Morel, F. M. M., Milligan, A. J., & Saito, M. A. (2003). Marine bioinorganic chemistry: The role of trace metals in the oceanic cycles of major nutrients. In *Treatise on geochemistry* (1st ed., Vol. 6, pp. 113–143). Elsevier.
- Moriyasu, R., Bolster, K. M., Hardisty, D. S., Kadko, D. C., Stephens, M. P., & Moffett, J. W. (2023). Meridional survey of the central Pacific reveals iodide accumulation in equatorial surface waters and benthic sources in the abyssal plain. *Global Biogeochemical Cycles*, *37*(3), e2021GB007300. <https://doi.org/10.1029/2021GB007300>
- Morse, J. W., & Luther, G. W. (1999). Chemical influences on trace metal-sulfide interactions in anoxic sediments. *Geochimica et Cosmochimica Acta*, *63*(19), 3373–3378. [https://doi.org/10.1016/S0016-7037\(99\)00258-6](https://doi.org/10.1016/S0016-7037(99)00258-6)
- Ohnemus, D. C., Rauschenberg, S., Cutter, G. A., Fitzsimmons, J. N., Sherrell, R. M., & Twining, B. S. (2016). Elevated trace metal content of prokaryotic communities associated with marine oxygen deficient zones. *Limnology & Oceanography*, *62*(1), 3–25. <https://doi.org/10.1002/lno.10363>
- Owens, S. A., Buesseler, K. O., & Sims, K. W. W. (2011). Re-evaluating the ²³⁸U-salinity relationship in seawater: Implications for the ²³⁸U–²³⁴Th disequilibrium method. *Marine Chemistry*, *127*(1), 31–39. <https://doi.org/10.1016/j.marchem.2011.07.005>
- Pearson, R. G. (1963). Hard and soft acids and bases. *Journal of the American Chemical Society*, *85*(22), 3533–3539. <https://doi.org/10.1021/ja00905a001>
- Plass, A., Schlosser, C., Sommer, S., Dale, A. W., Achterberg, E. P., & Scholz, F. (2020). The control of hydrogen sulfide on benthic iron and cadmium fluxes in the oxygen minimum zone off Peru. *Biogeosciences*, *17*(13), 3685–3704. <https://doi.org/10.5194/bg-17-3685-2020>
- Pos, W. H., Milne, P. J., Riemer, D. D., & Zika, R. G. (1997). Photoinduced oxidation of H₂S species: A sink for sulfide in seawater. *Journal of Geophysical Research*, *102*(D11), 12831–12837. <https://doi.org/10.1029/96JD03817>
- Radford-Knoery, J. (1993). *The biogeochemistry of hydrogen sulfide in the open ocean*. Old Dominion University.
- Radford-Knoery, J., & Cutter, G. A. (1993). Determination of carbonyl sulfide and hydrogen sulfide species in natural waters using specialized collection procedures and gas chromatography with flame photometric detection. *Analytical Chemistry*, *65*(8), 976–982. <https://doi.org/10.1021/ac00056a005>
- Radford-Knoery, J., & Cutter, G. A. (1994). Biogeochemistry of dissolved hydrogen sulfide species and carbonyl sulfide in the western North Atlantic Ocean. *Geochimica et Cosmochimica Acta*, *58*(24), 5421–5431. [https://doi.org/10.1016/0016-7037\(94\)90239-9](https://doi.org/10.1016/0016-7037(94)90239-9)
- Roshan, S., & DeVries, T. (2021). Global contrasts between oceanic cycling of cadmium and phosphate. *Global Biogeochemical Cycles*, *35*(6). <https://doi.org/10.1029/2021GB006952>
- Schlitzner, R. (2023). Ocean data view (5.6.5) [Computer Software]. <https://odv.awi.de>
- Schlosser, C., Streu, P., Frank, M., Lavik, G., Croot, P. L., Dengler, M., & Achterberg, E. P. (2018). H₂S events in the Peruvian oxygen minimum zone facilitate enhanced dissolved Fe concentrations. *Scientific Reports*, *8*(1), 12642. Article 1. <https://doi.org/10.1038/s41598-018-30580-w>
- Schmitt, A.-D., Galer, S. J. G., & Abouchami, W. (2009). Mass-dependent cadmium isotopic variations in nature with emphasis on the marine environment. *Earth and Planetary Science Letters*, *277*(1), 262–272. <https://doi.org/10.1016/j.epsl.2008.10.025>
- Sieber, M., Conway, T. M., de Souza, G. F., Obata, H., Takano, S., Sohrin, Y., & Vance, D. (2019). Physical and biogeochemical controls on the distribution of dissolved cadmium and its isotopes in the Southwest Pacific Ocean. *Chemical Geology*, *511*, 494–509. <https://doi.org/10.1016/j.chemgeo.2018.07.021>
- Sieber, M., Lanning, N. T., Bian, X., Yang, S.-C., Takano, S., Sohrin, Y., et al. (2023). The importance of reversible scavenging for the marine Zn cycle evidenced by the distribution of zinc and its isotopes in the Pacific Ocean. *Journal of Geophysical Research: Oceans*, *128*(4), e2022JC019419. <https://doi.org/10.1029/2022JC019419>
- Sieber, M., Lanning, N. T., Bunnell, Z. B., Bian, X., Yang, S.-C., Marsay, C. M., et al. (2023). Biological, physical, and atmospheric controls on the distribution of cadmium and its isotopes in the Pacific Ocean. *Global Biogeochemical Cycles*, *37*(2), e2022GB007441. <https://doi.org/10.1029/2022GB007441>
- Vance, D., de Souza, G. F., Zhao, Y., Cullen, J. T., & Lohan, M. C. (2019). The relationship between zinc, its isotopes, and the major nutrients in the North-East Pacific. *Earth and Planetary Science Letters*, *525*, 115748. <https://doi.org/10.1016/j.epsl.2019.115748>
- Vance, D., Little, S. H., de Souza, G. F., Khaliwala, S., Lohan, M. C., & Middag, R. (2017). Silicon and zinc biogeochemical cycles coupled through the Southern Ocean. *Nature Geoscience*, *10*(3), 202–206. <https://doi.org/10.1038/ngeo2890>
- Walsh, R. S., Cutter, G. A., Dunstan, W. M., Radford-Knoery, J., & Elder, J. T. (1994). The biogeochemistry of hydrogen sulfide: Phytoplankton production in the surface ocean. *Limnology & Oceanography*, *39*(4), 941–948. <https://doi.org/10.4319/lno.1994.39.4.0941>
- Weber, T., John, S., Tagliabue, A., & DeVries, T. (2018). Biological uptake and reversible scavenging of zinc in the global ocean. *Science*, *361*(6397), 72–76. <https://doi.org/10.1126/science.aap8532>
- Xie, R. C., Galer, S. J. G., Abouchami, W., & Frank, M. (2019). Limited impact of eolian and riverine sources on the biogeochemical cycling of Cd in the tropical Atlantic. *Chemical Geology*, *511*, 371–379. <https://doi.org/10.1016/j.chemgeo.2018.10.018>
- Xie, R. C., Le Moigne, F. A. C., Rapp, I., Lüdke, J., Gasser, B., Dengler, M., et al. (2020). Effects of ²³⁸U variability and physical transport on water column ²³⁴Th downward fluxes in the coastal upwelling system off Peru. *Biogeosciences*, *17*(19), 4919–4936. <https://doi.org/10.5194/bg-17-4919-2020>
- Xie, R. C., Rehkämper, M., Grasse, P., van de Fliedert, T., Frank, M., & Xue, Z. (2019). Isotopic evidence for complex biogeochemical cycling of Cd in the eastern tropical South Pacific. *Earth and Planetary Science Letters*, *512*, 134–146. <https://doi.org/10.1016/j.epsl.2019.02.001>
- Yang, J., Li, Y., Liu, S., Tian, H., Chen, C., Liu, J., & Shi, Y. (2015). Theoretical calculations of Cd isotope fractionation in hydrothermal fluids. *Chemical Geology*, *391*, 74–82. <https://doi.org/10.1016/j.chemgeo.2014.10.029>